Phospholipase C in Living Cells: Activation, Inhibition, Ca^{2+} Requirement, and Regulation of M Current

Lisa F. Horowitz,[1] Wiebke Hirdes,[1] Byung-Chang Suh,[1] Donald W. Hilgemann,[2] Ken Mackie,[1,3] and Bertil Hille[1]

[1]Department of Physiology and Biophysics, University of Washington School of Medicine, Seattle, WA 98195
[2]Department of Physiology, University of Texas Southwestern Medical Center at Dallas, Dallas, TX 75390
[3]Department of Anesthesiology, University of Washington School of Medicine, Seattle, WA 98195

We have further tested the hypothesis that receptor-mediated modulation of KCNQ channels involves depletion of phosphatidylinositol 4,5-bisphosphate (PIP_2) by phosphoinositide-specific phospholipase C (PLC). We used four parallel assays to characterize the agonist-induced PLC response of cells (tsA or CHO cells) expressing M_1 muscarinic receptors: translocation of two fluorescent probes for membrane lipids, release of calcium from intracellular stores, and chemical measurement of acidic lipids. Occupation of M_1 receptors activates PLC and consumes cellular PIP_2 in less than a minute and also partially depletes mono- and unphosphorylated phosphoinositides. KCNQ current is simultaneously suppressed. Two inhibitors of PLC, U73122 and edelfosine (ET-18-OCH_3), can block the muscarinic actions completely, including suppression of KCNQ current. However, U73122 also had many side effects that were attributable to alkylation of various proteins. These were mimicked or occluded by prior reaction with the alkylating agent N-ethylmaleimide and included block of pertussis toxin–sensitive G proteins and effects that resembled a weak activation of PLC or an inhibition of lipid kinases. By our functional criteria, the putative PLC activator *m*-3M3FBS did stimulate PLC, but with a delay and an irregular time course. It also suppressed KCNQ current. The M_1 receptor–mediated activation of PLC and suppression of KCNQ current were stopped by lowering intracellular calcium well below resting levels and were slowed by not allowing intracellular calcium to rise in response to PLC activation. Thus calcium release induced by PLC activation feeds back immediately on PLC, accelerating it during muscarinic stimulation in strong positive feedback. These experiments clarify important properties of receptor-coupled PLC responses and their inhibition in the context of the living cell. In each test, the suppression of KCNQ current closely paralleled the expected fall of PIP_2. The results are described by a kinetic model.

The Journal of General Physiology

INTRODUCTION

Recent work attributes the long-known muscarinic suppression of M-current K^+ channels (Brown and Adams, 1980) to a receptor-driven depletion of the trace membrane lipid phosphatidylinositol 4,5-bisphosphate (PIP_2) (Suh and Hille, 2002; Zhang et al., 2003; Ford et al., 2004; Winks et al., 2005). In this hypothesis, M-current channels require PIP_2 to function, and activation of M_1 muscarinic receptors results in destruction of PIP_2 via PIP_2-specific PLC. Our work seeks to strengthen the evidence for channel regulation by PIP_2 through a deeper understanding of the parameters of PLC activation and pharmacology in living cells and by asking if M-current modulation parallels PLC activation and PIP_2 hydrolysis under several conditions. Many cytoplasmic enzymes and cytoskeletal proteins become localized to membranes that contain PIP_2 (Lemmon, 2003), and activities of many kinds of membrane proteins, including ion channels and transporters, depend on PIP_2 levels in the plasma membrane (Hilgemann et al., 2001; Suh and Hille, 2005), so now there is renewed interest in understanding how PLC regulates phosphoinositide levels.

A large biochemical literature describes the signaling properties of phosphatidylinositol (PI)-specific PLCs in vitro (for review see Rhee, 2001). A few selected points given here are relevant for our work. This family of enzymes catalyzes the hydrolysis of PIP_2 to inositol 1,4,5-trisphosphate (IP_3) and diacylglycerol (DAG). The β isoform, PLCβ, is activated by G protein–coupled receptors that couple through G proteins of the G_q family by direct action of $G\alpha_qGTP$ (Smrcka et

L.F. Horowitz, W. Hirdes, and B.-C. Suh contributed equally to this work.

Correspondence to Bertil Hille: hille@u.washington.edu

L.F. Horowitz's present address is Fred Hutchinson Cancer Research Center, 1100 Fairview Ave N., Seattle, WA 98109.

W. Hirdes's present address is Institut für Angewandte Physiologie, Universitätsklinikum Hamburg-Eppendorf, Universität Hamburg, D-20246 Hamburg, Germany.

The online version of this article contains supplemental material.

Abbreviations used in this paper: CHO, Chinese hamster ovary; DAG, diacylglycerol; EGFP, enhanced green fluorescent protein; IP_3, inositol 1,4,5-trisphosphate; mRFP, monomeric red fluorescent protein; NEM, N-ethylmaleimide; oxo-M, oxotremorine-M; PH, pleckstrin homology; PIP_2, phosphatidylinositol 4,5-bisphosphate.

al., 1991), and PLCβ can also be activated by G protein βγ subunits (Rhee, 2001). Stimulation of G_q-coupled receptors in intact cells usually results in intracellular Ca^{2+} release mediated by gating of IP_3 receptors, which may be followed by additional Ca^{2+} influx from the extracellular space. In test tube studies, the stimulation of PLC depends on the local calcium concentration $[Ca^{2+}]$ according to a broad, bell-shaped curve with a maximum between 10 and 100 μM Ca^{2+} (Ryu et al., 1987b). In spite of considerable efforts, the pharmacology of PLCs remains poorly developed and controversial. Many papers show that several isoforms of PLC are inhibited by the aminosteroid compound U73122 and not by its "inactive" analogue U73343 (Smith et al., 1990). It is also inhibited by the ether lipid analogue edelfosine (ET-18-OCH_3) (Powis et al., 1992). Finally, a recent report says that several isoforms of PLC are activated by the benzenesulfonamide *m*-3M3FBS and not by its inactive analogue *o*-3M3FBS (Bae et al., 2003), but the specificity of this action has been disputed (Krjukova et al., 2004).

Here we are interested in the in vivo properties of PLC as they affect phosphoinositide metabolism and KCNQ current. We use three nondestructive, continuous monitors to follow the activity of PLC during stimulation by transfected M_1 muscarinic receptors or by *m*-3M3FBS in intact tsA-201 cells, and we use a biochemical assay of phospholipids in Chinese hamster ovary (CHO) cells. The M_1 receptor pathway uses $G_{q/11}$ in tsA-201 cells (Hirdes et al., 2004; Suh et al., 2004) and hence should selectively stimulate PLCβ isoforms. Activation of PLC is monitored with a confocal fluorescence microscope by observing two optical probes that track depletion of PIP_2 and production of IP_3 and DAG. These widely used translocation probes migrate between the cell membrane and cytoplasm during PLC activity. They are fusions of enhanced green fluorescent protein (EGFP) with the PIP_2- and IP_3-binding pleckstrin homology (PH) domain of PLCδ1 or with the DAG-binding PKC cysteine-rich homology-1 domain, C1A (PKC-C1; Oancea et al., 1998; Stauffer et al., 1998; Várnai and Balla, 1998). In addition, downstream effects of PLC are monitored optically with a Ca^{2+}-sensitive fluorescent dye that reports the IP_3-dependent release of Ca^{2+} from intracellular stores and Ca^{2+} entry from the medium. Further, we assay the relative sizes of various phospholipid pools by biochemical methods. Finally, parallel measurements are made of M current as expressed from KCNQ2 and KCNQ3 channel subunits (KCNQ2/3 current).

Our paper asks the following questions. Is PIP_2 depleted by activation of M_1 receptors, and to what extent do the different reporters of PIP_2 monitor the same signal? What are the consequences and mechanism of inhibition by U73122? What are the parameters of activation by *m*-3M3FBS? Can PLC be activated at cellular resting levels of cytoplasmic $[Ca^{2+}]_i$? Is it speeded significantly by $[Ca^{2+}]_i$ elevations, and is it slowed by $[Ca^{2+}]_i$ reductions? Does this regulation affect whether PIP_2 can be depleted significantly in the plasma membrane during receptor activation? Do changes of KCNQ2/3 current mirror changes of PIP_2?

MATERIALS AND METHODS

Cell Culture and Transfection

Human embryonic kidney tsA-201 (tsA) cells were cultured and transiently transfected using Lipofectamine 2000 (Invitrogen) with various cDNAs (Suh et al., 2004): M_1-muscarinic receptor (1 μg, from Neil Nathanson, University of Washington, Seattle, WA), PH-PLCδ1-EGFP (PH-EGFP, 0.25 μg, from P. De Camilli, HHMI, Yale University, New Haven, CT), PKC-C1A-EGFP (C1-EGFP, 0.25 μg, from T. Meyer, Stanford University, Stanford, CA), PH-PLCδ1-mRFP (PH-mRFP, 0.25 μg, from C. Kearn, University of Washington, using mRFP from Roger Tsien, University of California, San Diego, CA), inositol 1,4,5-trisphosphate-5-phosphatase (IP_3-5-P, 2 μg, from M. Iino, University of Tokyo, Japan), the channel subunits KCNQ2 and KCNQ3 (Kv7.2 and Kv7.3, 1 μg, from David McKinnon, State University of New York, Stony Brook, NY), RGS-2 (2 μg, Guthrie Research Institute, Sayre, PA), and GFP (0.1 μg) as a marker for transfection. TsA cells were maintained in DMEM (Invitrogen) supplemented with 10% FCS and 0.2% penicillin/streptomycin. In a few electrophysiological experiments we used the mouse AtT-20 neuroendocrine cell line, which expresses endogenous M_4 muscarinic receptors and G protein–coupled inward rectifiers (GIRK channels). They were grown in DMEM supplemented with 10% horse serum and 0.2% penicillin/streptomycin. For biochemical experiments we used a line of CHO cells stably transfected with M_1-muscarinic receptors (CHO-M1 from N.J. Buckley and D.A. Brown, University College, London, UK). They were grown in F-12K nutritional mixture with 10% bovine calf serum and 1% penicillin/streptomycin.

Reagents

The muscarinic receptor agonist oxotremorine-M (oxo-M) was used at 10 μM. Chemicals were purchased from Sigma-Aldrich, except U73122 (1-[6-[[17 β-3-methoxyestra-1,3,5(10)-trien-17-yl]amino]hexyl]-1H-pyrrole-2,5-dione) and U73343 (Research Biochemicals), BAPTA-AM and BAPTA (Molecular Probes), *m*-3M3FBS (2,4,6-trimethyl-N-(meta-3-trifluoromethyl-phenyl)-benzene-sulfonamide) and *o*-3M3FBS (Tocris), and edelfosine (Calbiochem).

Confocal Imaging and Analysis

TsA cells were imaged 24–48 h after transfection on poly-L-lysine–coated coverslips (Suh et al., 2004). The external Ringer's solution used for confocal observations and for current recording contained (in mM): 160 NaCl, 2.5 KCl, 2 $CaCl_2$, 1 $MgCl_2$, 10 HEPES, and 8 glucose, adjusted to pH 7.4 with NaOH. Images were taken every 5 s on a Leica TCS/MP confocal microscope at room temperature and processed with Metamorph (UIC) and Igor Pro 4.0 (Wavemetrics, Inc.). To obtain averaged time courses, the fluorescence intensity F over a given region of the cytoplasm or nucleus was usually normalized to the average intensity for the 30 s before agonist application F_0 (F/F_0). Images are shown here in negative contrast so that the brightest fluorescence appears black.

Electrophysiology and Calcium Photometry

TsA cells were whole-cell clamped at room temperature 24–48 h after transfection (Suh et al., 2004). The pipette solution contained (in mM): 175 KCl, 5 $MgCl_2$, 5 HEPES, 0.1 BAPTA, 3 Na_2ATP, 0.1 Na_3GTP, pH 7.4 adjusted with KOH. For the experiments of Fig. 8 (E and F), the pipette solution was sometimes supplemented with 10 mM calcium, 1 μM thapsigargin, 100 μg/ml pentosan polysulfate (an IP_3 receptor blocker; Bezprozvanny et al., 1993), and more BAPTA as described. The special pipette solution with 10 mM $CaCl_2$ and 20 mM BAPTA has an estimated free $[Ca^{2+}]$ of 128 nM. When measuring the rates of induction and recovery from muscarinic inhibition of the current, we applied test and control solutions rapidly to the 100 μl chamber (flow rate of 1.5 ml min^{-1}) in the vicinity of the recorded cell. The solutions exchanged in ~6 s. Recordings were performed using a HEKA EPC-9 amplifier with Pulse software (HEKA Elektronik). Data analysis was done using Igor Pro 4.0. Cells were held at a holding potential of −20 mV, and 500-ms test pulses to −60 mV were given every 4 s. Reported values ($I_{-20\ mV}$) are mean outward current taken at −20 mV just before each step to −60 mV. Recordings started ~5 min after breakthrough. Some experiments studied inward rectifier currents in AtT-20 cells, which were recorded using the same pipette solution but with a bath solution where the Na^+ and K^+ concentrations were changed to 125 Na^+ and 40 K^+. For photometry, cells were preloaded with indo-1-AM (Molecular Probes) and not subjected to patch clamp. The ratio of background-corrected 405/505 nm emission elicited by excitation at 365 nm was used to calculate absolute $[Ca^{2+}]_i$ levels (Shapiro et al., 2000).

Analysis of Acidic Membrane Lipids

Membrane lipids of CHO-M1 cells were analyzed as previously described (Nasuhoglu et al., 2002a). In brief, acidic phospholipids were extracted and deacylated to give the parent glycero-headgroups, which were then separated by HPLC and detected by suppressed conductivity. The relative quantity of each headgroup is expressed as the percentage of all acidic lipid headgroups.

Student's unpaired *t* test (2 tailed), or, when indicated, a one-way ANOVA with a Bonferroni post-hoc test for multiple comparisons, was used to test for significance. Where error bars are shown, they represent SEM

Online Supplemental Material

The supplemental material for this paper comprises one figure and the listing of a computer program (available at http://www.jgp.org/cgi/content/full/jgp.200509309/DC1). Fig. S1 shows changes in the voltage dependence of activation of KCNQ current caused by addition of U73122 or N-ethylmaleimide. The computer program describes the elementary model for translocation of PH-EGFP and C1-EGFP probes between cytoplasm and nucleus.

RESULTS

Two Translocation Probes Report Activation of PLC via M_1 Receptors

We start with control experiments to understand the properties of our two translocation probes. Fig. 1 A shows the M_1 receptor–mediated activation of PLC as seen with the PH-EGFP probe (top) and the C1-EGFP probe (bottom) in separate cells before, during, and after a 3-min application of the muscarinic agonist oxo-M (10 μM). The closed green lines outline a cytoplasmic region of interest and the red lines, a nuclear region of interest. Since the PH-EGFP has affinity for PIP_2 and IP_3, it binds to the PIP_2 in the plasma membrane at rest (dark cell outline in first frame), translocates to the cytoplasm as oxo-M stimulation of PLC causes IP_3 to rise in the cytoplasm and PIP_2 to fall at the membrane (darkened cytoplasm in second frame), and returns to the plasma membrane after oxo-M is washed off while IP_3 is being hydrolyzed and PIP_2 resynthesized (last frame). The rise and fall of cytoplasmic PH-EGFP fluorescence is reversible and repeatable (Fig. 1 B, green). Similar experiments with the C1-EGFP probe, which binds to DAG, show a reciprocal time course of translocation. That probe is uniformly distributed in the cytoplasm and nucleus at rest (dark cytoplasm in Fig. 1 A and symbols in Fig. 1 C), reporting little DAG on any membrane, but migrates to the plasma membrane as oxo-M stimulation of PLC produces DAG there, and returns to the cytoplasm when oxo-M removal allows DAG to decline. Oxo-M affects the two probes with approximately equal potency, giving midpoints for peak translocation near 0.25 and 0.28 μM oxo-M (Fig. 1, D and E). The initial migration takes 10–15 s (Fig. 1, B and C; points are 5 s apart), and the recovery takes 100–200 s.

The cytoplasmic concentration change of both probes sags during the 3-min-long application of oxo-M (Fig. 1, B and C) as if there were some kind of desensitization and reversal of the PLC response. This implied that there might be some unexpected features to PIP_2 metabolism. However, further analysis suggests that the sag is at least partly caused by an additional slow exchange of probe molecules between the nucleus and cytoplasm. Compare the thin red traces of nuclear fluorescence in Fig. 1 (B and C) with the heavier green traces of cytoplasmic fluorescence. At rest, the nuclear and cytoplasmic concentrations are similar. During repeated stimulation and wash, the nuclear fluorescence starts to rise after the cytoplasmic fluorescence rises, and to fall after the cytoplasmic fluorescence falls. The same can be seen in the pictures of Fig. 1 A, where the nuclear and cytoplasmic fluorescence are about equal at rest (Fig. 1 A, top left), and early in the oxo-M treatment the nucleus (clear disk inside cell) remains much lighter than the cytoplasm, but after washout of oxo-M, the nucleus remains a little darker than before (Fig. 1 A, top right). Simple modeling (see APPENDIX and Fig. 11) shows that the nuclear fluorescence tracks the cytoplasmic fluorescence with an exponential relaxation time constant τ of ~360 or 225 s (for PH-EGFP and C1-EGFP, respectively), equivalent to nuclear envelope permeability coefficients of 0.0025 or 0.004 μm s^{-1}. Slow exchange with the nucleus accounts for perhaps half of the sag of the response during oxo-M, for most of the observed overshoot in the recovery of C1-EGFP after oxo-M is removed, and for the significant background

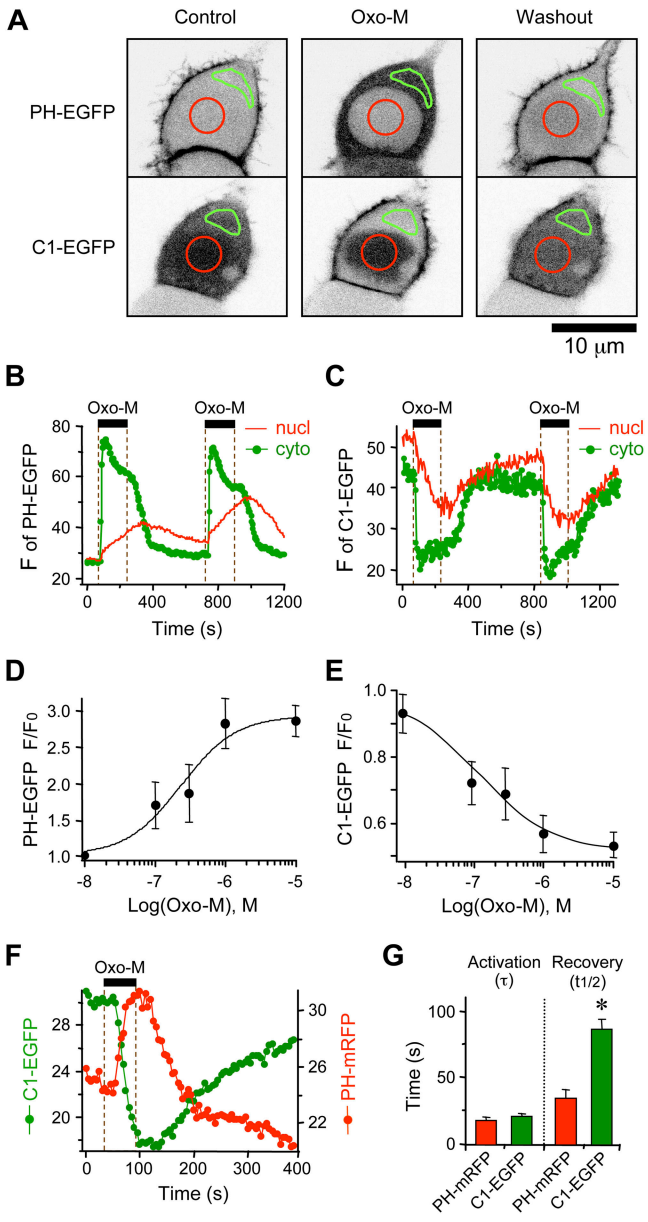

Figure 1. Oxo-M translocates two complementary optical probes of PI metabolism. (A) Confocal images of the PH-EGFP or C1-EGFP probes transiently expressed in separate tsA cells, shown in negative contrast (fluorescence is dark). Cells (both presumably recently divided) before oxo-M, after 50 s of 10 μM oxo-M, and after 200 s of washout. The optical sections pass through the nucleus, which is centered in the frame and has a red circular region of interest. The cytoplasm has a green region of interest. (B) Time course (5-s sample intervals) of mean fluorescence per pixel in a cytoplasmic (green line and symbols) and a nuclear region-of-interest (red line) of a cell during two 3-min applications of oxo-M with the PH-EGFP probe (different cell from A). (C) Cytoplasmic and nuclear fluorescence in a similar experiment, but with the C1-EGFP probe. (D) Dose–response relation for translocation of the PH-EGFP probe. Cytoplasmic fluorescence (F) relative to fluorescence at the beginning of the experiment (F_0) for n = 4–6 cells per point. (E) Dose–response experiments with the C1-EGFP probe, n = 4–8 cells per point. Here F_0 is the last measured control point before each oxo-M application. (F) Representative time courses of cytoplasmic translocation (5-s sample intervals) for C1-EGFP (green) and PH-mRFP (red) measured simultaneously at two wavelengths in the same cell. (G) Exponential time constant for translocation (τ) during oxo-M application and half-time for recovery after washout (n = 5). *, P = 0.016 indicates significant difference from the recovery rate of PH-mRFP.

level of cytoplasmic and nuclear PH-EGFP before oxo-M and of C1-EGFP during oxo-M. Thus the background level can be described as an equilibrium distribution of probe rather than as a nonspecific binding.

The nearly reciprocal movement of the two probes is highlighted in Fig. 1 F, which is from a simultaneous two-color fluorescence measurement in one cell. For this experiment, the PH domain is fused to a monomeric red fluorescent protein (mRFP), and the C1 domain probe is fused to green EGFP. As the red fluorescent protein was more subject to photobleaching with our illumination settings, it shows a superimposed gradual decline over the 400-s period. In a series of two-color experiments with these probes, the exponential time constants for initial translocation and the half times for fluorescence recovery for oxo-M are τ_{trans} = 16 ± 2 s and $t_{1/2\ rec}$ = 36 ± 6 s for PH-mRFP (n = 5) and τ_{trans} = 19 ± 1 s and $t_{1/2\ rec}$ = 87 ± 7 s for C1-EGFP (n = 5) (Fig. 1 G). The initial translocation time is similar, but recovery of the C1-EGFP probe is significantly slower than that of the PH-mRFP probe. However, there is no a priori expectation that the recoveries would be similar since the metabolic pathways that dephosphorylate IP_3, synthesize more PIP_2, and phosphorylate DAG are different and independent.

The Inhibitor U73122 Has Complex Actions

U73122 is a PLC inhibitor that is widely used as a quick test for the involvement of PLC in a signaling pathway. In our experiments, U73122 strongly uncoupled activation of PLC by receptors as expected. Fig. 2 (A and B) shows confocal experiments with U73122 and its relatively inactive analogue U73343 using the DAG probe (C1-EGFP). Again, oxo-M is applied twice for 3 min. The DAG probe translocates to the membrane during the first oxo-M application, but not after a 5-min application of U73122 (2.5 μM; Fig. 2 A; n = 10). The control compound U73343 seems inactive as it does not prevent the translocation (Fig. 2 B; n = 3). These robust effects seem readily interpreted as a simple inhibition of M_1 receptor–stimulated PLC activation and DAG production. In these experiments, U73122 by itself tends to augment the cytoplasmic fluorescence of the DAG probe in resting cells as if it has released some of the probe from the membrane (Fig. 2 A).

Similar experiments with the IP_3/PIP_2 probe (PH-EGFP) suggest a more complicated picture (Fig. 2, C and D). Again, U73122 fully blocks the translocation induced by oxo-M; however, even without oxo-M, U73122

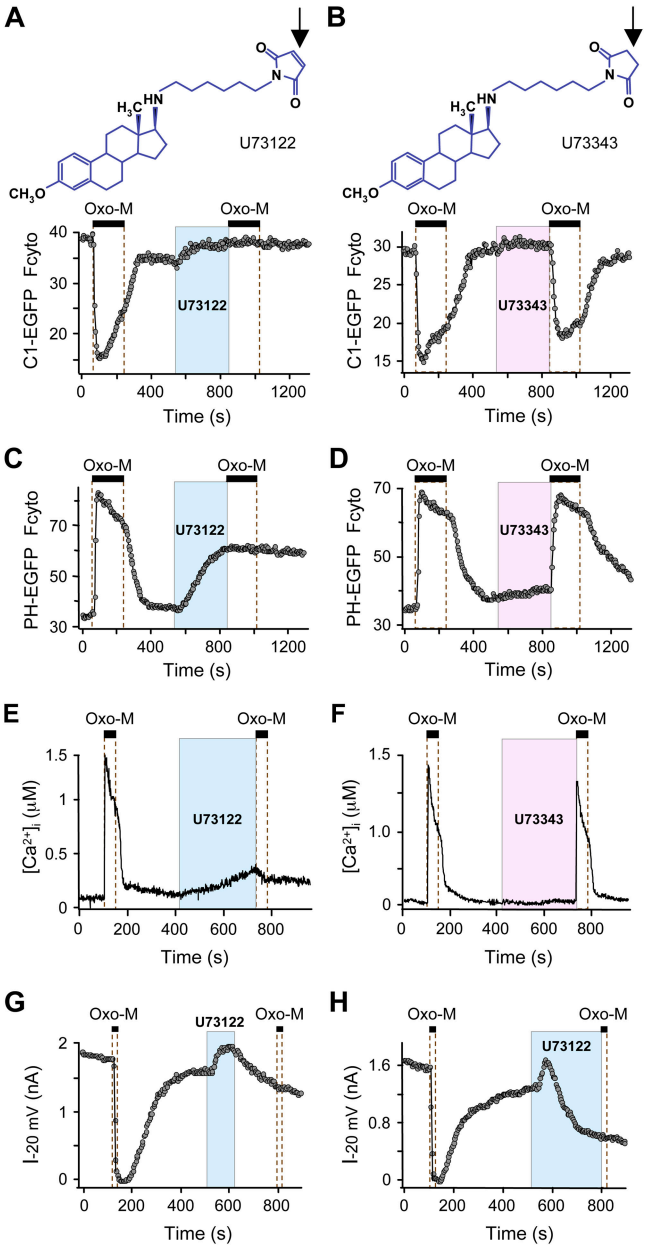

Figure 2. U73122 blocks the muscarinic translocation of two optical probes, intracellular calcium responses, and modulation of KCNQ current. All traces are representative experiments from single cells. (A and B) Time courses of cytoplasmic fluorescence in representative confocal translocation experiments with the C1-EGFP probe before and during perfusion of oxo-M (10 μM, 3 min), first without and then with 5-min treatments with 2.5 μM U73122 (A) or U73343 (B). Insets show the structure of these compounds. (C and D) Similar confocal experiments in cells expressing the PH-EGFP probe and using 3 μM U73122 or U73343. (E and F) Indo-1 photometry Ca^{2+} measurements showing block by U73122 but not U73343 of oxo-M (60 s) induced $[Ca^{2+}]_i$ elevations. (G and H) Electrophysiological experiments (4-s sample intervals) showing action of 3 μM U73122, 2 min application (G) or 5 min application (H), on KCNQ2/3 current and its modulation by oxo-M.

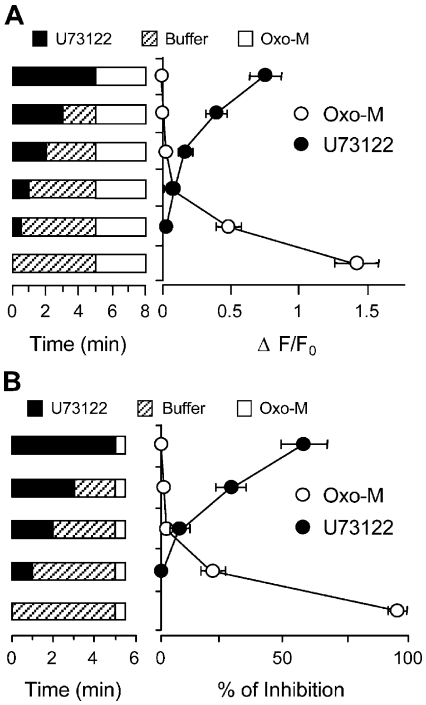

Figure 3. Time course of actions of U73122. (A) Cells are preexposed to U73122 for 0, 0.5, 1, 2, 3, or 5 min and to 5, 4.5, 4, 3, 2, or 0 min of control solution before a 3-min application of oxo-M. Bars show this protocol of treatments. Increment in cytoplasmic PH-EGFP fluorescence measured at 5 min (at the end of the preexposure period and before the oxo-M; filled circles) and the additional increment of fluorescence after oxo-M application (open circles). (B) Cells are preexposed to U73122 for 0, 1, 2, 3, or 5 min and to 5, 4, 3, 2, or 0 min of control solution before a 30-s application of oxo-M. Depression of KCNQ current measured at 5 min and the additional suppression of current after oxo-M application.

initiates a slow translocation of the probe (Fig. 2 C; n = 15 cells). This translocation is 30 times slower than that with oxo-M. As expected, the control compound U73343 does not block oxo-M action (Fig. 2 D; n = 7), although in some experiments at high concentration, U73343 by itself seemed to induce a slight translocation. Translocation occurs with U73122 alone even when the extracellular solution includes no calcium (unpublished data; n = 7). These observations suggest the working hypothesis that U73122 efficiently blocks activation by the G_q pathway, as is widely reported, but it is also a very weak agonist of PLC. Fig. 3 A examines the time course of these effects. U73122 (3 μM) was applied for 0, 0.5, 1, 2, 3, or 5 min. According to the PIP_2/IP_3 probe, receptor-induced activation of PLC is half blocked after just 0.5 min of 3 μM U73122, whereas the U73122-induced translocation of probe (closed symbol) takes significantly longer, and is half induced after 3 min of U73122.

Calcium photometry measurements are consistent with our working hypothesis (Fig. 2, E and F). A first application of oxo-M raises $[Ca^{2+}]_i$ strongly. The initial

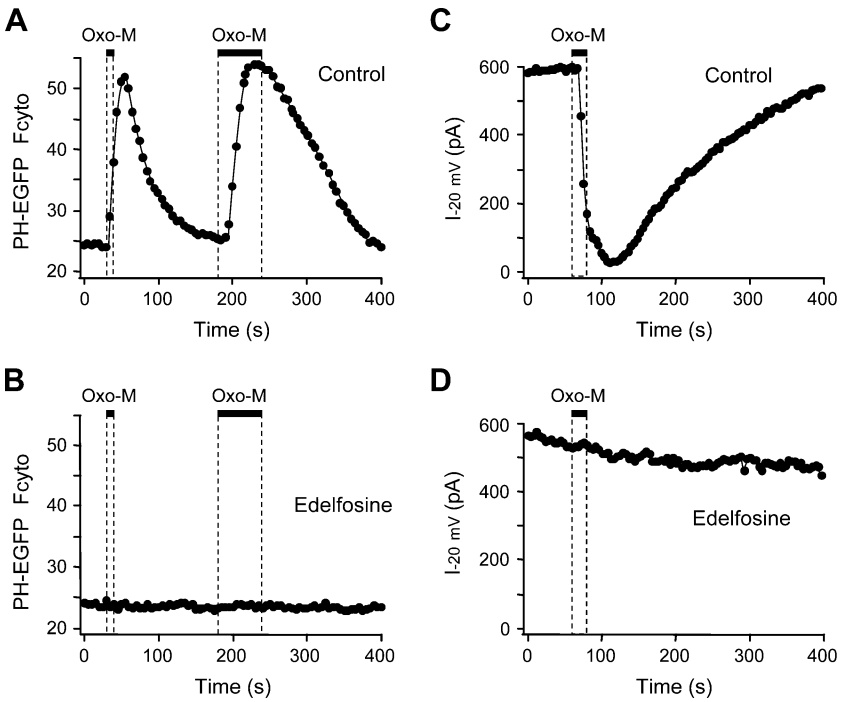

Figure 4. Edelfosine blocks PLC activation. Cells were preincubated with vehicle or 10 μM edelfosine for 30 min at 37°C and then used in the experiment. Data are representative of three to five separate experiments for cells stimulated with 10 μM oxo-M. (A and B) Translocation of the PH-EGFP probe in control (A) or edelfosine-treated (B) cells. (C and D) Modulation of KCNQ2/3 current in control (C) or edelfosine-treated (D) cells.

calcium rise comes from intracellular stores, presumably by IP_3-dependent release, but the later plateau requires extracellular calcium (unpublished data; $n = 5$ cells) and probably involves calcium entry that depends on store emptying. Induction of $[Ca^{2+}]_i$ elevations by agonist is fully blocked after prior exposure to U73122 (Fig. 2 E; $n = 5$) but not after the inactive analogue U73343 (Fig. 2 F; $n = 4$). Nevertheless, U73122 alone raises $[Ca^{2+}]_i$ a little, albeit very slowly (Fig. 2 E; $n = 6$).

Experiments with KCNQ2/3 current give a similar picture (Fig. 2, G and H). Fig. 2 G shows the expected suppression of current by oxo-M (measured at −20 mV) and its prevention by U73122. The initial control application of oxo-M for 30 s strongly suppresses current as PLC is activated and PIP_2 is depleted (Suh and Hille, 2002; Suh et al., 2004). The suppression is reversible. The time course of this current modulation is reminiscent of the time course of PIP_2 hydrolysis reported by the PH-EGFP probe (Fig. 2 C), although the recovery of current is consistently a little slower than the recovery of PH-EGFP distribution. Next, when U73122 is applied for 2 min, the current starts to increase rapidly, an unexpected result, and then to decline steadily below the initial level. Subsequent application of oxo-M is ineffectual, indicating again that M_1 receptor coupling to PLC has been powerfully blocked (Fig. 2 G, $n = 5$). With a 5-min application of U73122, the initial augmentation is similar but the current declines considerably during the exposure to the inhibitor (Fig. 2 H, $n = 12$). Fig. 3 B examines the time course of these effects. U73122 (3 μM) was applied for 1, 2, 3, 4, or 5 min. The block of receptor coupling (open symbols) is almost complete after a 1-min exposure to U73122, and the U73122-induced depression of current (closed symbols) is still only partial after 3 min of U73122.

Why does the current increase and then decrease during U73122? We begin with the transient augmentation, which Stemkowski et al. (2002) have also described for endogenous M current in frog sympathetic neurons. We asked if it could be due to a changed voltage dependence of activation by measuring the amplitudes of tail currents at −70 mV after 500-ms depolarizations to different test potentials. Indeed, this protocol revealed that U73122 shifts the voltage dependence of KCNQ2/3 channel activation to more negative potentials by 14 ± 3 mV ($n = 4$; see Fig. S1 A, available at http://www.jgp.org/cgi/content/full/jgp.200509309/DC1). Such a shift would allow more channels to open at −20 mV since steady-state activation at that voltage is normally incomplete (only 52%) and would be increased to 80% by the drug (Fig. S1 A). The subsequent decline of current is consistent with the hypothesis that U73122 acts as a very weak agonist of PLC, resulting in a slow decline in the membrane PIP_2 and hence of the current. Again, the rate of decline is ∼30 times slower than the rapid suppression by oxo-M, suggesting that PLC is turned on to only 3–4% of the maximum level achieved with receptor activation.

The actions of U73122 were sufficiently complex that we wanted to test another inhibitor of PLC. We tried the lipid-like, anti-neoplastic agent edelfosine (ET-18-OCH_3). As is shown in Fig. 4 (A and B), this compound (10 μM for 30 min) entirely prevented the muscarinic

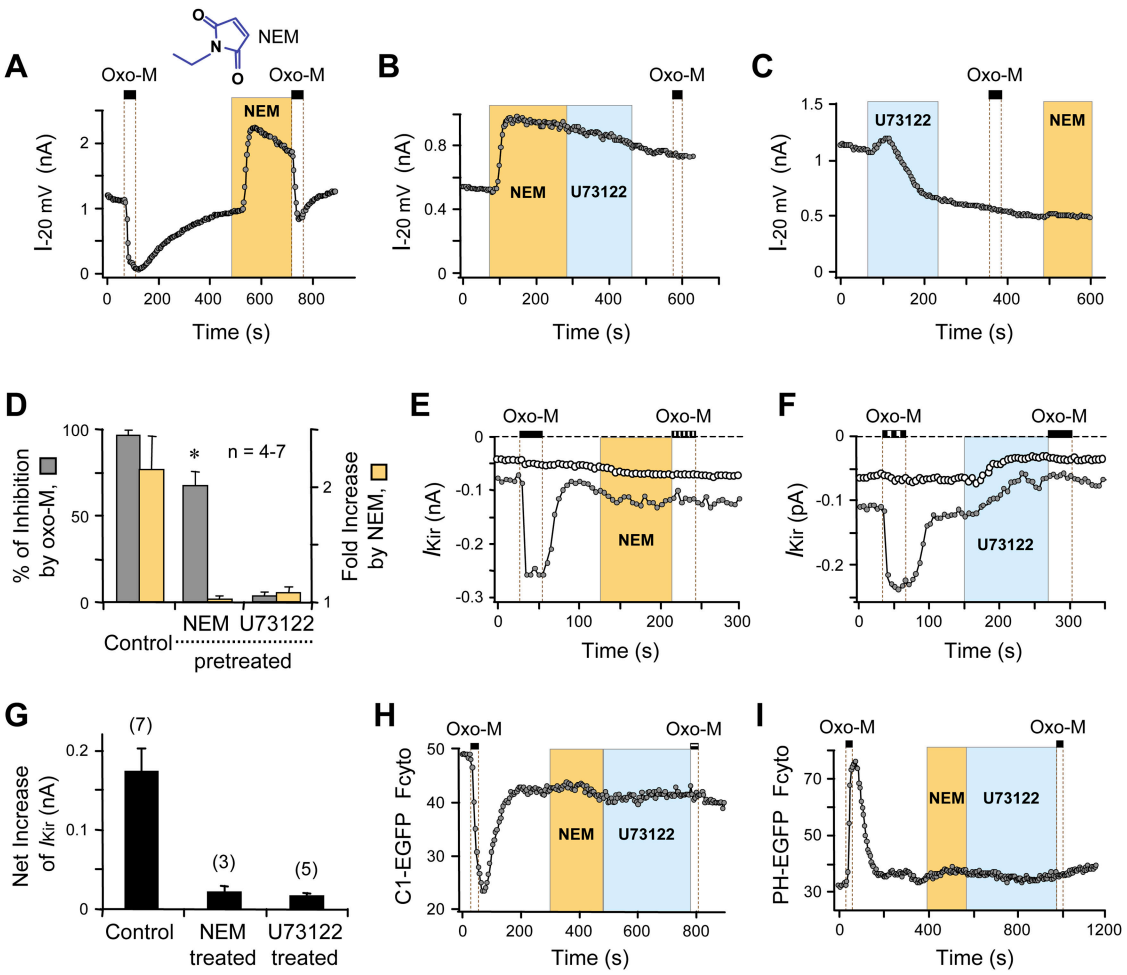

Figure 5. NEM mimics or occludes several actions of U73122. NEM is applied at 100 μM for 120 s and U73122 is applied at 3 μM throughout. All traces are for representative single cells. (A–D) KCNQ2/3 current in tsA cells and its modulation by oxo-M. (A) NEM alone. Inset shows structure of NEM. (B) NEM followed by U73122. (C) U73122 followed by NEM. (D) Summary of A–C. Left axis is percent inhibition of KCNQ current by oxo-M application. Right axis is fold increase of KCNQ current with NEM application. The cells were untreated or pretreated with NEM or U73122. *, $P < 0.05$, compared with control. (E–G) Inward rectifier K current at −100 mV (filled circles) and holding current at −40 mV (open circles) in AtT-20 cells. (E) Effect of NEM. (F) Effect of U73122. (G) Summary of K^+ current increase. Number of cells is given in parentheses. (H and I) Cytoplasmic fluorescence of translocation probes C1-EGFP (H) and PH-EGFP (I) during NEM, U73122, and oxo-M.

translocation of the PH-EGFP probe and the muscarinic inhibition of KCNQ currents (at 15 min the action of edelfosine was strong but incomplete). Furthermore, by itself it did not induce the rise and inhibition of KCNQ current or the slow migration of the PH-EGFP probe seen with U73122. These actions of edelfosine are consistent with simple inhibition of PLC, and we interpret the additional effects of U73122 as side effects with other mechanisms.

Some Actions of U73122 May Represent Alkylation

The literature on U73122 contains numerous suggestions of side effects that could not be attributed to simple block of PLC (see DISCUSSION). We decided to investigate the initial augmentation of KCNQ current with U73122 as such a side effect. The only structural difference between U73122 and U73343 is one double bond (Fig. 2, A and B, insets) that makes U73122 chemically reactive. U73122 is an N-substituted maleimide, which like N-ethylmaleimide (NEM) should be able to alkylate cysteine −SH groups, tethering the entire U73122 compound covalently to the cysteine. U73343 is the corresponding unreactive succinimide. Both the augmentation of KCNQ current and the negative shift of activation with U73122 reminded us of augmentations and shifts induced by NEM acting on cysteine residues of KCNQ channels (Roche et al., 2002; Li et al., 2004). We verified that the shifts are quite similar (Fig. S1 B). Therefore we sought to test the hypothesis that U73122 can act as a hydrophobic- or membrane-targeted version of NEM, capable of reacting with −SH groups generally.

Fig. 5 A shows powerful augmentation of KCNQ2/3 current by 120 s of 100 μM NEM, as previously reported (Roche et al., 2002). The augmentation is consistently larger than that with U73122. Somewhat like U73122, NEM also slows and decreases the subsequent response to oxo-M; however, this effect is only partial. Fig. 5 B shows that prior NEM treatment prevents U73122 from augmenting KCNQ current and also from subsequently decreasing it, but prior NEM does not prevent U73122 from fully uncoupling receptor activation from PLC. Similarly, prior U73122 treatment prevents NEM for augmenting KCNQ current (Fig. 5 C). The effects summarized in Fig. 5 D suggest that both the augmentation and the subsequent decline of current with U73122 are side effects dependent on alkylating accessible −SH groups. As expected for such reactions, all actions of NEM and of U73122 were irreversible on the time scale of our experiments.

As a further test of the alkylation hypothesis, we asked if U73122 mimics another effect of NEM on signaling to ion channels. Previously we have shown that NEM readily blocks electrophysiological responses due to pertussis toxin–sensitive G proteins (G_i/G_o), presumably by alkylating the same G protein cysteine residue that pertussis toxin ADP ribosylates (Shapiro et al., 1994). One such response is the pertussis toxin–sensitive opening of inward rectifier GIRK channels by muscarinic agonists acting on M_2 receptors (Pfaffinger et al., 1985). Fig. 5 E shows that oxo-M acting via endogenous M_4 receptors activates this inward current in AtT-20 cells, and that NEM completely uncouples the muscarinic effect as was expected from block of G_i/G_o. Similarly, U73122 uncouples the M_4 muscarinic action (Fig. 5 F; see summary Fig. 5 G) even though PLC is not involved. Again, U73122 mimics an effect of NEM, this time on pertussis toxin–sensitive G proteins. Treatment with U73122 also reduces the holding current somewhat.

Our last example of occlusion of U73122 actions by NEM returns to the translocation probes. Prior treatment with NEM eliminates the small augmentation of cytoplasmic fluorescence by U73122 seen with C1-EGFP (Fig. 5 H; $n = 4$; compare with Fig. 2 A) and the large slow augmentation seen with PH-EGFP (Fig. 5 I; $n = 7$; compare with Fig. 2 C). Thus by many criteria, U73122 and NEM mimic and occlude each others' actions. However, NEM did not occlude one action of U73122; namely, it did not prevent U73122 from fully uncoupling muscarinic activation of PLC as judged by the translocation assays ($n = 11$). In addition, by itself NEM did not induce translocation of either probe, even with a 5-min treatment (unpublished data).

Phosphoinositides Are Hydrolyzed

We undertook an analysis of acidic phospholipids of CHO-M1 cells during treatments with carbachol, U73122, and NEM. These cells express M_1 receptors stably. Using deacylated headgroups, our method measures the relative abundance of six acidic lipids: phosphatidylinositol (PI), phosphatidylinositol 4-phosphate (PIP), PIP_2, phosphatidylserine, cardiolipin, and phosphatidic acid (Nasuhoglu et al., 2002a). Fig. 6 reports PI, PIP, and PIP_2 as percent of the total of the six acidic lipid classes measured. In unstimulated cells, PI is almost 50% of the total and PIP and PIP_2 are only ~1% each, truly trace phospholipids. A 1-min carbachol treatment strongly reduces PIP_2 and PIP (to 7% and 12% of control, respectively) and slightly but significantly reduces PI (to 95% of control), consistent with a powerful muscarinic activation of PLCβ depleting the major cellular pools of PIP_2. A 5-min treatment with 5 μM U73122 alone also reduces PIP_2 and PIP, although not as much as carbachol, and it renders subsequent treatment with carbachol ineffectual. These results would be consistent with a weak activation of PLC by U73122, and a total block of carbachol action. Alternative interpretations are considered in DISCUSSION.

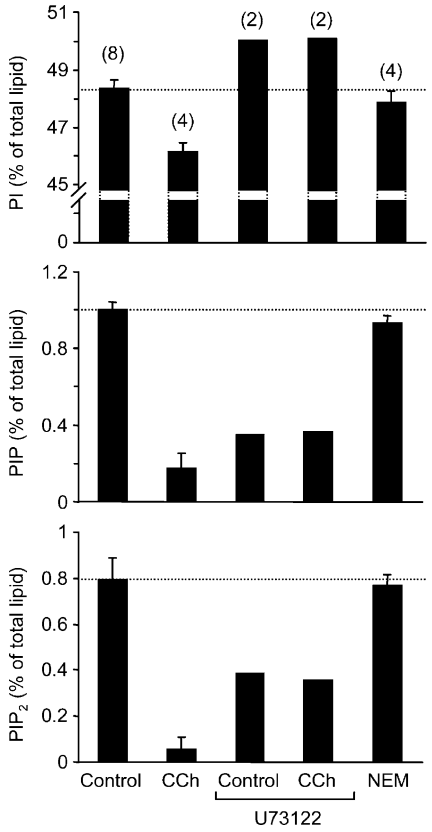

Figure 6. Carbachol and U73122 decrease PIP_2. Size of PI, PIP, and PIP_2 pools in CHO-M1 cells expressed relative to the sum of six acidic phospholipids. Treatments were: none (Control), 1 min of 200 μM carbachol (CCh), 5 min of 5 μM U73122 (U73122 Control), U73122 followed by 1 min of carbachol with U73122 (U73122 CCh), and 2 min of 100 μM NEM. Number of cells is given in parentheses.

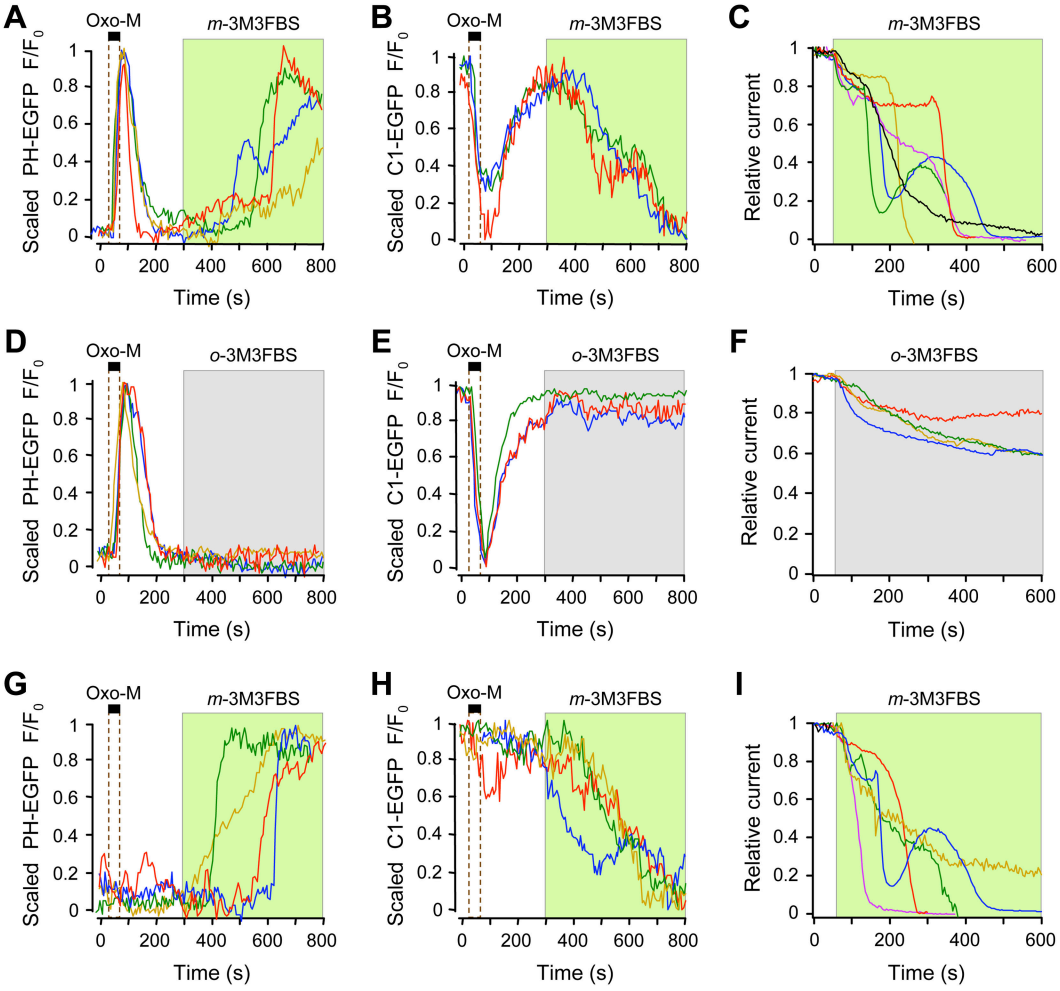

Figure 7. *m*-3M3FBS stimulates PLC. Panels show time courses for each of three to six individual cells of scaled cytoplasmic fluorescence of PH-EGFP (A, D, and G) Scaled cytoplasmic fluorescence of C1-EGFP (B, E, and H) and relative KCNQ2/3 current (C, F, and I). To scale the fluorescence, each record was normalized to its own maximum and minimum. (A–C) Cells treated with oxo-M and then with 50 μM *m*-3M3FBS. (D–F) Cells treated with oxo-M and then with 50 μM *o*-3M3FBS. (G–I) Cells were cotransfected with RGS2 protein (24 h) and then treated with oxo-M followed by 50 μM *m*-3M3FBS.

NEM did not change the lipid composition in 2 min, but in further measurements not shown, it did reduce PIP_2 and PIP by 35 and 50%, respectively, in 5 min. Also we mention that both PIP and PIP_2 levels consistently rebounded ~50% back toward control levels after 10 min in the continued presence of agonist.

Since the stable CHO-M1 cells used for chemical assays were different from the tsA cells used in the rest of our experiments, we checked the oxo-M–induced modulation of KCNQ2/3 current and the translocation of the PH-EGFP probe in them. The speed and amplitude of the muscarinic current modulation and of the probe migration were virtually identical to those in tsA cells, where the M_1 receptor had been introduced by transient transfection (n = 5–8). We conclude that the quantitative parameters of KCNQ2/3 current inhibition and PI metabolism are indistinguishable in the two cell lines.

m-3M3FBS Activates PLC with a Delay

In search of other practical ways to activate PLC, we then studied the putative PLC activator *m*-3M3FBS and its control compound *o*-3M3FBS (Bae et al., 2003). We found that the meta compound causes migration of the PH-EGFP and C1-EGFP probes (Fig. 7, A and B), and it induces suppression of the KCNQ2/3 current (Fig. 7 C). By these criteria, it activates PLC. Judging from the relative steepness of the traces, the apparent activation by *m*-3M3FBS is relatively strong once it starts but is still a little weaker than for the maximal activation by oxo-M. The action begins abruptly after a variable delay of several hundred seconds and sometimes it reverses spontaneously for 200 s, only to start up again. The control compound *o*-3M3FBS induces no migration of the probes and no suppression of current beyond the usual rundown that would be seen in control conditions (Fig. 7, D–F). In our previous work, we have

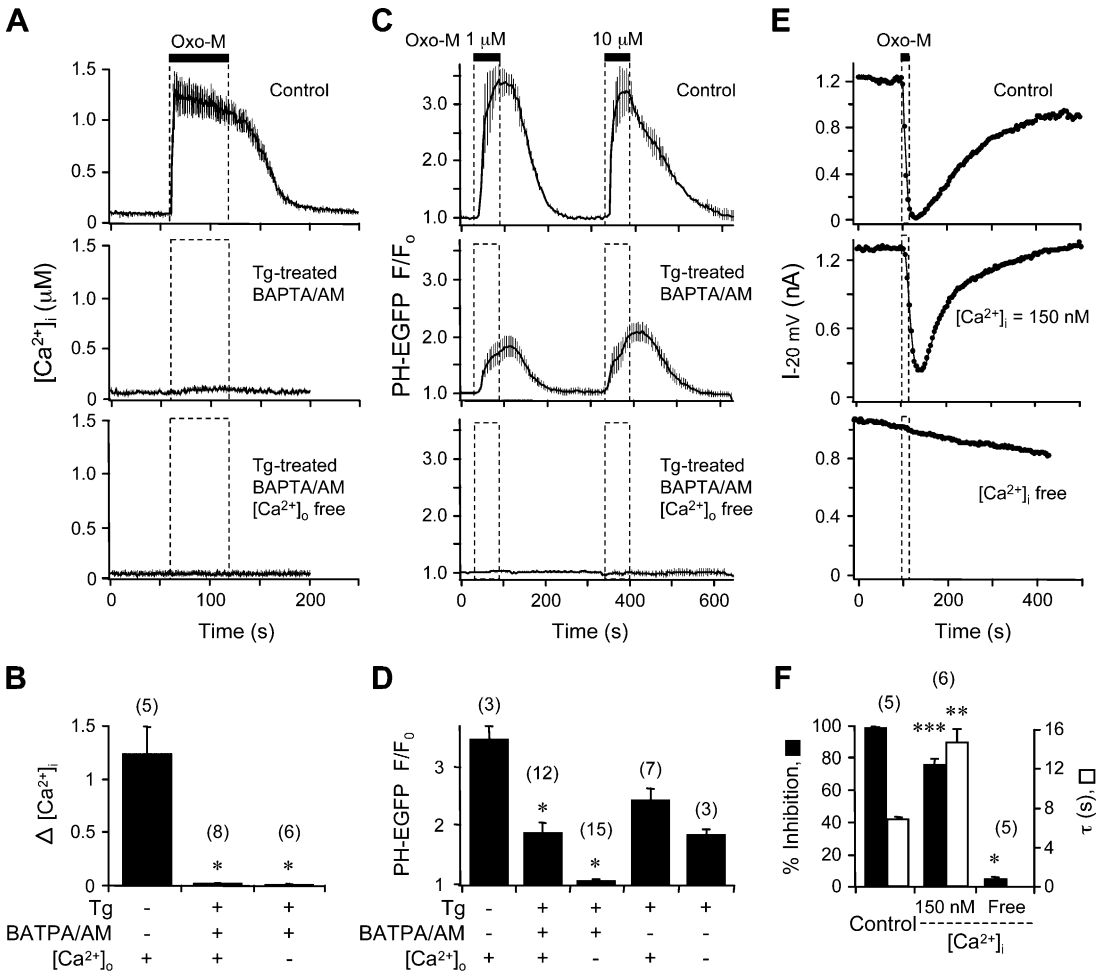

Figure 8. Buffering $[Ca^{2+}]_i$ depresses muscarinic activation of PLC. (A) Oxo-M-evoked $[Ca^{2+}]_i$ rises with different intracellular Ca^{2+} buffering: no exogenous buffer (top) or pretreatment with thapsigargin (20 min, 1 μM) and loaded with BAPTA-AM (50 μM for 20 min) either in the presence of extracellular Ca^{2+} (2 mM) (middle) or in the absence of extracellular Ca^{2+} (plus 0.5 mM EGTA) (bottom). (B) Means of experiments as in A. *, $P < 0.001$, compared with control. (C) Oxo-M–induced cytoplasmic fluorescence increases (PH-EGFP) under the same three buffering conditions as in A. (D) Means of experiments as in C and two additional sets using no BAPTA/AM to buffer $[Ca^{2+}]_i$. *, $P < 0.001$, compared with control. (E) Oxo-M–induced suppression of KCNQ2/3 current with different intracellular Ca^{2+} buffers in the whole-cell pipette: 0.1 BAPTA (top); 20 BAPTA + 10 $CaCl_2$ + 100 μg/ml PPS (middle); or 20 BAPTA + 0 $CaCl_2$ (bottom). The middle and lower cells were also pretreated with 1 μM thapsigargin. (F) Mean amplitude of inhibition and time constant (τ) for current suppression; τ for calcium-free condition not determined. *, $P < 0.001$, compared with % inhibition of control. **, $P < 0.01$, compared with τ of control. ***, $P < 0.05$, compared with % inhibition of control.

shown that coexpression of the $G_{q/11}$-specific regulator of G protein signaling RGS-2 blocks oxo-M–induced migration of PH-EGFP and suppression of KCNQ2/3 current in these cells (Suh et al., 2004). This is evidence that the normal muscarinic action via M_1 receptors requires participation of the G protein $G_{q/11}$. Coexpression of RGS-2 does not block the activation of PLC by *m*-3M3FBS (Fig. 7, G–I). Hence the activator must work downstream of muscarinic receptors and G_q.

PLC Needs Calcium

We explored the $[Ca^{2+}]_i$ dependence of the muscarinic activation of PLC by buffering cellular $[Ca^{2+}]_i$ to different levels. The principal questions were whether PLC in live cells can be activated when Ca^{2+} is well below normal, whether the IP_3-induced release of Ca^{2+} from intracellular stores exerts positive feedback to accelerate PLC, and whether modulation of KCNQ current has the same calcium dependence.

The experiments in Fig. 8, A, C, and E, each include three different intracellular conditions. In the top panels, $[Ca^{2+}]_i$ is relatively unbuffered (control). In the middle panels, $[Ca^{2+}]_i$ is strongly buffered under conditions intended to mimic and stabilize resting levels. In the lower panels, $[Ca^{2+}]_i$ is strongly buffered using conditions intended to clamp it well below normal resting levels. In the photometry and confocal experiments (Fig. 8, A–D), which used intact cells, the Ca^{2+} buffer-

ing was achieved by preloading membrane-permeant BAPTA-AM and by pretreating with thapsigargin to allow any intracellular stores to empty. The $[Ca^{2+}]_i$ level was manipulated by doing these incubations and the subsequent measurements either in 2 mM Ca^{2+}–containing or Ca^{2+}-free solutions (with EGTA). As expected, the $[Ca^{2+}]_i$ measurements (Fig. 8, A and B) showed that $[Ca^{2+}]_i$ rises briskly after the muscarinic stimulus when it is unbuffered, and it does not rise significantly when it is strongly buffered at either normal or subnormal levels. The confocal experiment (Fig. 8, C and D) showed that, relative to controls, the oxo-M–induced translocation of PH-EGFP still occurs but is slowed and reduced in final amplitude when $[Ca^{2+}]_i$ is buffered at resting levels. Prior emptying of intracellular Ca^{2+} stores with thapsigargin without buffering internal Ca^{2+} with BAPTA/AM reduces subsequent oxo-M–induced translocation of PH-EGFP to a similar extent (Fig. 8 D). Translocation is nearly absent when $[Ca^{2+}]_i$ is held at reduced levels (Fig. 8 C, bottom). Together, these experiments show that muscarinic activation of PLC requires some free Ca^{2+}. PLC can be activated at resting $[Ca^{2+}]_i$ levels, but activation is potentiated considerably (positive feedback) when IP_3 is allowed to elevate $[Ca^{2+}]_i$ above the resting level. This positive feedback occurs in <5 s.

Finally, we measured modulation of KCNQ2/3 current under these three calcium conditions. Since the electrophysiology experiments were done with whole-cell clamp, the Ca^{2+} buffers were introduced via the recording pipette (see MATERIALS AND METHODS and legend). The current measurements (Fig. 8, E and F) show that KCNQ2/3 current is quickly and completely suppressed after a 20-s exposure to oxo-M if $[Ca^{2+}]_i$ is left unbuffered ($\tau = 7 \pm 0.3$ s, $n = 5$; inhibition = 98 ± 2%); it is more slowly and less completely suppressed if $[Ca^{2+}]_i$ is kept at resting levels ($\tau = 14.3 \pm 1.6$ s, $n = 6$; inhibition = 75 ± 4%); and it is unaffected by oxo-M if $[Ca^{2+}]_i$ is kept below normal (inhibition = 4 ± 2%, $n = 5$). Thus the calcium dependence of signaling to KCNQ current parallels that of PLC activation.

Does Ca^{2+} entry play a role in regulating PLC as well? An enhancement of the $[Ca^{2+}]_i$ rise and of PLC activity by extracellular calcium is evident in experiments with longer exposures to oxo-M (Fig. 9). Consider the time course of $[Ca^{2+}]_i$ during 180-s oxo-M exposures as extracellular Ca^{2+} is altered. Fig. 9 (A–C) shows $[Ca^{2+}]_i$ responses to two successive oxo-M applications. In the control condition, oxo-M evokes a transient elevation of $[Ca^{2+}]_i$ >1 μM that decays to a plateau of several hundred nanomolar until oxo-M is removed. The second application evokes a similar, often slightly less robust, response with the standard bathing medium (Fig. 9 A; $n = 15$) but a smaller transient and no plateau if

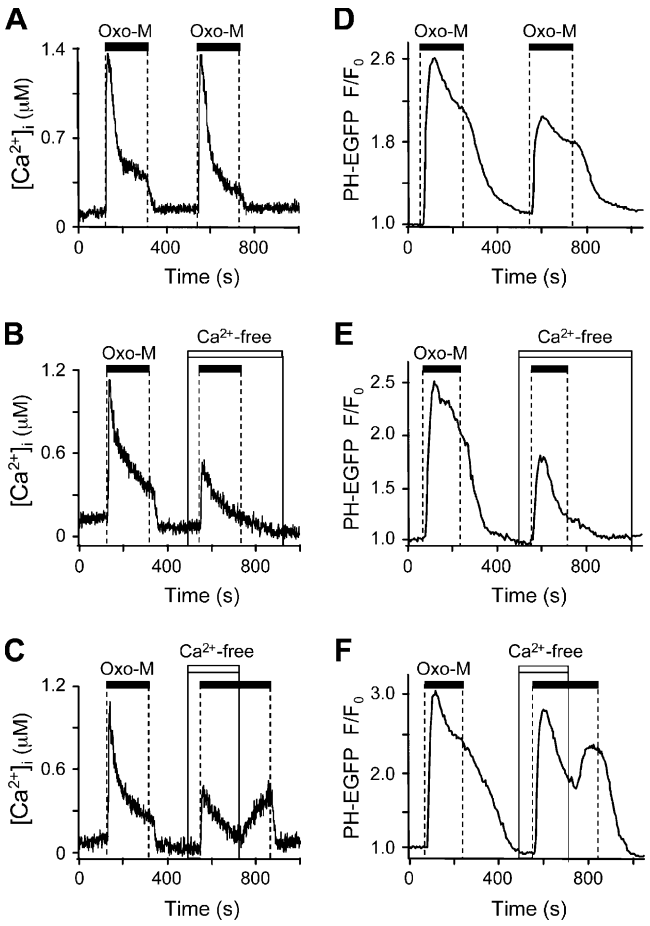

Figure 9. Store-operated Ca^{2+} entry potentiates activation of PLC. (A–C) Time course of $[Ca^{2+}]_i$ increase during two applications of oxo-M (black bars). Each record from a single cell. The bath contains 2 mM Ca^{2+} most of the time, except during white bars in B and C when it is a Ca^{2+}-free solution with 0.5 mM EGTA. (D–F) Mean time course of rise of normalized cytoplasmic fluorescence of PH-EGFP during two applications of oxo-M (n = 4–6, SEM not shown ranges from 5–20%). Bath solutions as in A–C.

done in Ca^{2+}-free medium (Fig. 9 B; $n = 5$). If the medium Ca^{2+} is restored partway through the oxo-M exposure, the $[Ca^{2+}]_i$ rises up again (Fig. 9 C; $n = 5$). These observations are the signatures of a late, store-operated Ca^{2+} entry. Apparently oxo-M induces an initial transient release of intracellular Ca^{2+} that in tsA cells is followed by opening of store-operated channels on the plasma membrane. These plasma membrane channels maintain the $[Ca^{2+}]_i$ plateau, but shut quickly after agonist is removed. Fig. 9 (D–F) shows translocation of the IP_3/PIP_2 probe, PH-EGFP, in parallel experiments. The records resemble those of the $[Ca^{2+}]_i$ transients. Namely, the translocation is decidedly attenuated and decays more rapidly when the bath has Ca^{2+}-free solution (Fig. 9 F; $n = 4$), and it is augmented if Ca^{2+} is restored while oxo-M is still being applied (Fig. 9 E; $n = 4$). Thus, the activity of PLC is significantly increased

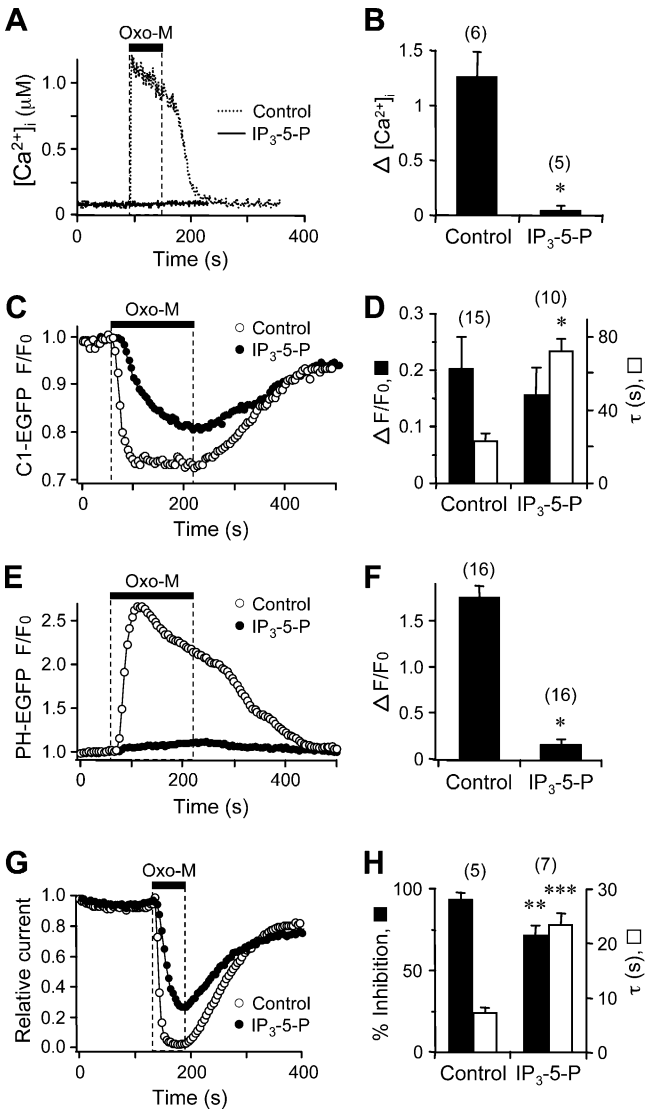

Figure 10. The IP_3 pathway potentiates activation of PLC. Each left panel shows experiments on a representative control cell and a representative cell transfected 24–48 h earlier with IP_3-5-phosphatase (IP_3-5-P), and the right panel shows means of 5–16 cells. (A and B) Time course and peak $[Ca^{2+}]_i$ rise during a 1-min application of oxo-M. *, $P < 0.001$, compared with control. (C and D) Time course, amplitude, and time constant of KCNQ2/3 current inhibition during 1-min applications of oxo-M. **, $P < 0.01$, compared with % inhibition of control. ***, $P < 0.01$, compared with τ of control. (E and F) Time course, amplitude, and time constant of decrease of cytoplasmic C1-EGFP fluorescence during 3-min applications of oxo-M. *, $P < 0.001$, compared with τ of control. (G and H) Time course and peak amplitude of increase of cytoplasmic PH-EGFP fluorescence during 3-min applications of oxo-M. *, $P < 0.001$, compared with control.

not only by IP_3-evoked Ca^{2+} release but also by the subsequent store-operated Ca^{2+} entry.

We used one more approach to test the calcium dependence of muscarinically activated PLC. By overexpression of the enzyme, type I IP_3-5-phosphatase (IP_3-5-P), which catalyzes the first step in IP_3 degradation, we could abort the PLC-generated rise of IP_3 concentration and consequently the IP_3-induced elevation of $[Ca^{2+}]_i$. Fig. 10 (A and B) shows that expression of IP_3-5-P effectively eliminates the muscarinic $[Ca^{2+}]_i$ transient, presumably because IP_3 is degraded as soon as it is made. Further, Fig. 10 (C–F) shows that expression of IP_3-5-P slows and decreases the muscarinic translocation of the DAG probe, C1-EGFP, and the PIP_2/IP_3 probe, PH-EGFP. These two measures report that the PLC response is weakened but not abolished when IP_3 buildup and Ca^{2+} release are prevented. They suggest that PIP_2 is only partially depleted by 3 min of oxo-M when IP_3-5-P prevents the positive feedback by Ca^{2+}. With the PH-EGFP probe there is almost no translocation when IP_3-5-P is expressed. Presumably, the combination of some unhydrolyzed PIP_2 remaining in the plasma membrane and no IP_3 accumulating in the cytoplasm means that the PH-EGFP probe remains membrane bound. The final experiment measures muscarinic suppression of KCNQ2/3 current for comparison with the observations on PLC. The suppression is slow and only partial in the IP_3-5-P cells, as expected if PLC is slowed, PIP_2 is cleaved more slowly, and much PIP_2 remains.

Morphological Effects of our Reagents

We report here briefly several consistent additional effects of our reagents on the morphology of the tsA cells. When oxo-M was perfused onto cells, successive 5-s images show considerable agitation in the cell surface region. The membrane appears to be bubbling out in blebs and small extensions. Presumably this motion reflects local breakdown of the actin cytoskeleton and perhaps an arrest of endocytosis as plasma membrane PIP_2 becomes depleted (Rohrbough and Broadie, 2005). A second set of observations is that application of U73122 slowly causes cells to round up irreversibly and occasionally leads to an abrupt enhancement of nuclear envelope permeability indicated by a sudden diffusion of the optical probes into the nucleus (<5 s); NEM induces blebbing; and edelfosine slowly induces cell swelling (although KCNQ current remains) and eventual lysis. NEM also strongly blocks diffusional exchange of probes between the nucleus and cytoplasm as if it closes nuclear pores.

DISCUSSION

Comparison with Previous Observations on PIP_2 and PLC

We have used three functional assays and one biochemical assay to monitor the effects of PLC on phosphoinositide metabolism. The concordance of the results obtained with all methods validates their use and strengthens our conclusions. All approaches agreed that activation of endogenous PLC, presumably mostly

the β-isoform(s), by M_1 receptors expressed in tsA and CHO-M1 cells strongly depletes both the functional plasma membrane PIP_2 and the total cellular PIP_2 in less than 1 min, producing IP_3-dependent Ca^{2+} release and DAG. According to the translocation probes, the majority of free cellular PIP_2 is confined to the plasma membrane, and DAG, which is initially not abundant, is produced primarily in the plasma membrane. The rapid and powerful depletion of PIP_2 and considerable depletion of PIP agree well with biochemical measurements in the SH-SY5Y human neuroblastoma cell line (Willars et al., 1998) and contrast with observations in heart and cell cultures in which G_q/PLC-coupled receptors may be less prevalent (Nasuhoglu et al., 2002b). The results show that the cells we used have a large endogenous reserve of PLC activity that can couple to introduced receptors. We find that KCNQ2/3 channel activity closely follows the overall changes of PIP_2 in response to a wide range of treatments. KCNQ current is therefore a sensitive and useful indicator of PIP_2 that appears to report global PIP_2 levels rather than a private "local pool" in these experiments.

We have published a kinetic model containing tentative estimates of the time course of phosphoinositide turnover following M_1 receptor activation (Suh et al., 2004). The model considered plasma membrane PI, PIP, and PIP_2 and four principal enzymes of phosphoinositide metabolism: a PI-4-kinase to make PIP from PI, a PI(4)P-5-kinase to make PIP_2 from PIP, a PI(4,5)P_2-5-phosphatase to reverse the former step, and a PIP_2-specific PLC that hydrolyzes PIP_2. Calculations with that model predict severe depletion of PIP_2, with only 0.66% remaining for a 60-s exposure to 10 μM oxo-M, and moderate depletion of PIP, with 40% remaining. On the other hand, using a chemical assay, we now find that 7% of total cellular PIP_2 and only 12% of the PIP remain under these conditions (Fig. 6). How can these differences be reconciled? We start with PIP_2. Some fraction of the total cellular PIP_2 may not be readily accessible to the PLC that is activated by M_1 receptors and G_q because this fraction resides on membranes other than the plasma membrane or is very tightly sequestered or segregated from PLC. For example, PIP_2-binding proteins and lipid rafts might be able to remove PIP_2 from the accessible pool (Yin and Janmey, 2003) such that this PIP_2 fraction is not hydrolyzed in the first minute. Nevertheless, in terms of this concept of distinct pools of lipids we have to conclude that at least 93% of the total cellular PIP_2 and 88% of the PIP form large accessible pools at the plasma membrane, suggesting that any other functional pools that may exist are small. The large pool of PIP_2 is reported by KCNQ current and by translocation of PH domain probes.

What about the greater-than-predicted loss of PIP, also reported by Willars et al. (1998)? In our model, a small depletion of PIP arises because the combination of PI(4)P-5-kinase and PI(4,5)P_2-5-phosphatase acts in a cycle to make PIP partially dependent on PIP_2 by feedback via PI(4,5)P_2-5-phosphatase. The decline of PIP could be speeded and intensified in the model by speeding both enzymes of this cycle, making PIP more tightly coupled to PIP_2. However, another more likely possibility is that PLCβ can hydrolyze PIP in addition to PIP_2, contrary to many current descriptions. Early in vitro biochemical experiments with vesicles containing PI, PIP, or PIP_2 led Wilson et al. (1984) and Ryu et al. (1987a) to propose that PLC hydrolyzes PI, PIP, and PIP_2 in a Ca^{2+}-dependent manner. If we neglect complications of separate pools, our model could deplete the PIP to a steady state of 12% (as observed) by assuming that PLC hydrolyzes PIP with a rate constant that is 1/7 of that for PIP_2. The predicted depletion is relatively fast with a time constant of 14 s. (See APPENDIX for further analysis of the Suh et al., 2004, model.) If, however, we introduce an inaccessible pool of PIP, then the rate constant of PIP hydrolysis would have to be made more similar to that for PIP_2.

Comparison with Previous Observations on Calcium and PLC

Our functional assays concur in finding that in the living cell, the activation of PLCβ by M_1 receptors is slowed if $[Ca^{2+}]_i$ is not permitted to rise above resting levels and is stopped if $[Ca^{2+}]_i$ is kept well below resting levels. The activation is greatest if an IP_3-dependent Ca^{2+} release occurs that is allowed to raise the $[Ca^{2+}]_i$ to micromolar levels. Store-operated entry of Ca^{2+} from the outside also can contribute to maintaining PLC activity, but stops as soon as the receptor agonist is removed. The positive feedback by calcium is significant. When it is permitted, the activation of PLC may become 10–15-fold greater than when it is not permitted, according to our model. These properties make PLCβ a coincidence detector that responds strongly to simultaneous activation of receptors and rise of Ca^{2+} (Hashimotodani et al., 2005). For example, a postsynaptic membrane with colocalized Ca^{2+}-permeable ionotropic glutamate receptors and G_q-coupled metabotropic glutamate receptors might activate PLC powerfully.

This calcium dependence agrees well with the reported in vitro calcium dependence curve for PLCβ (Ryu et al., 1987b; Smrcka et al., 1991; Biddlecome et al., 1996). It also agrees qualitatively with previous experiments reporting an arrest of receptor-stimulated phosphoinositide turnover when digitonin- or electropermeabilized cells are exposed to EGTA, and an acceleration when exposed to solutions with elevated calcium (Fisher et al., 1989; Wojcikiewicz et al., 1994). The reports known to us indicate that the phosphoinositide PLC enzyme activity falls virtually to zero in the ab-

sence of Ca^{2+}, and the rates of hydrolysis by G_q-activated PLCβ are strongly sensitive to Ca^{2+} in the region around the 100 nM typical resting concentration. The experiments with permeabilized cells agree that calcium concentrations achieved during cell signaling do not activate the β isoforms of PLC by themselves. However, calcium is a requirement for PLCβ activation by G_q. It remains to be established whether PLCs besides PLCβ become involved in the response amplification by Ca^{2+}. The crystal structure of mammalian PLCδ has an essential Ca^{2+} ion in the active site that can coordinate with one of the phosphate groups of the substrate (Essen et al., 1996), and that isoform is an excellent candidate for direct activation by physiological Ca^{2+} signals, in particular by nearby plasma membrane Ca^{2+} channels (Kim et al., 1999).

Optical Probes as Indicators of PI Metabolism

The behavior of the PH-EGFP and C1-EGFP probes in our study fits well with their original description as probes of PIP_2/IP_3 and of DAG (Oancea et al., 1998; Stauffer et al., 1998; Várnai and Balla, 1998; Hirose et al., 1999). Both probes clearly have access to the nucleus, and they undergo a slow, NEM-sensitive exchange between nucleus and cytoplasm when the probe concentration differs between these two compartments. This exchange seems symmetrical and passive. It adds transient components to the time course of cytoplasmic probe, which so far as we know have not been recognized previously. The transients fit a simple three-compartment, passive model. The diffusion of unfused EGFP through nuclear pores of COS-7 cells has been studied by fluorescence recovery after photobleaching. In those cells, diffusional exchange of EGFP (27 kD) is characterized by a time constant and nuclear membrane permeability of $\tau = 164$ s and $P_{nuc} = 0.011\ \mu m\ s^{-1}$ (Wei et al., 2003). For the larger C1-EGFP probe (34 kD) we found $\tau = 188$ s and $P_{nuc} = 0.005\ \mu m\ s^{-1}$, and for PH-EGFP (41 kD), $\tau = 281$ s and $P_{nuc} = 0.0032\ \mu m\ s^{-1}$ (see Fig. 11 and calculations in APPENDIX and computer program in online supplemental material). These diffusion properties fit well with the concept of lower permeability for a larger molecule, giving the expected permeability sequence EGFP > C1-EGFP > PH-EGFP.

There has been some argument whether PH-EGFP might be viewed as a pure PIP_2 probe or as a pure IP_3 probe, despite being able to bind to both compounds. One line of argument used to support a pure "IP_3 hypothesis" was that the measured affinity for IP_3 is 10–20 times higher than for PIP_2 (Lemmon et al., 1995; Hirose et al., 1999). In our discussion of the kinetic model of Suh et al. (2004) in APPENDIX, we conclude that our results and other published work with the PH domain probe in cells are not compatible with the large difference in affinity measured by binding studies on purified components. A second argument for this hypothesis was that IP_3 will displace PH domains from PIP_2-containing cell membranes (Hirose et al., 1999), but in all cases the amount of IP_3 needed exceeds that expected in cells (see APPENDIX). A third argument was that expression of the enzyme IP_3-5-P can stop migration of the probe despite activation of PLC (Okubo et al., 2004), as we also found. It was presumed that the only change with IP_3-5-P expression was that IP_3 did not accumulate. However, we have now shown that this maneuver stops calcium feedback to PLC and in our case slowed it so much that PIP_2 hydrolysis was no longer complete. Thus we suggest that experiments with IP_3-5-P do not settle the argument. We prefer the viewpoint that the PH probe responds to both the PIP_2 precursor and the IP_3 product, and during an experiment their relative importance changes as their relative concentrations change. This approach is suggested by the results of Xu et al. (2003) and Winks et al. (2005).

Does *m*-3M3FBS Activate PLC?

We had hoped to develop other practical ways to activate PLC for our experiments. Agonist properties of *m*-3M3FBS had been discovered in a large chemical screen against responses of neutrophils (Bae et al., 2003). It was reported to enhance superoxide production, increase intracellular Ca^{2+}, promote IP_3 production, and to activate purified PLCs of the β, γ, and δ classes directly in vitro. The effects were not sensitive to pertussis toxin or to expression of RGS2. A later work found a Ca^{2+} rise but could not confirm activation of PLC either chemically or with the PH-EGFP translocation probe (Krjukova et al., 2004). In our work, we have seen all the effects expected for an activator of PLC (translocation of PH-EGFP, translocation of C1-EGFP, and decrease of KCNQ2/3 current) and conclude that 50 μM *m*-3M3FBS does activate PLC relatively strongly. However, it is slow to act, has a variable long latency, and a fluctuating response. The ebb and flow of translocation probes and current with *m*-3M3FBS suggest that conflicting signal systems are activated and the balance sometimes favors turning on PLC and sometimes, turning off. In the end, PLC turns on in our conditions. Perhaps in other cells and under different application conditions the putative turning-off process might win. Variability of response, photolability, fluorescence, and spectral overlap with the common Ca^{2+} indicator fura-2 (Jansen et al., 2004) could limit the applicability of this compound in experiments with intact cells.

U73122 and Alkylation

PubMed lists over 1,500 papers with U73122 in the abstract. The large majority use the inhibitor simply as a

tool to check that some signaling pathway requires PLC. However, numerous papers report additional unexpected effects, raising question whether this agent can be used as a pharmacological tool without serious side effects. We select results from just four early papers. The initial brief announcement of U73122 from Upjohn reports that it inhibits partially purified PLC in vitro when the molar ratio of Ca^{2+}:PI in the assay was <2, but "increased PLC activity" when the molar ratio was 4–12 (Bleasdale et al., 1989). There are no data or experimental details in that book chapter. A careful study in NG108-15 neuroblastoma-glioma cells and in dorsal root ganglion cells shows that U73122 blocks bradykinin-induced Ca^{2+} transients irreversibly with a steep dose–response curve and a half-effective dose IC_{50} of 200 nM for 20-min preincubations and that U73343 is without effect (Jin et al., 1994). However, these authors also find a slow rise of intracellular Ca^{2+} in Ca^{2+}-free bath solutions and a total block of L-type Ca^{2+} channels. They mention the possibility of protein alkylation for such side effects. A study of the amount and isotopic labeling of phosphoinositide pools in platelets found 50% reduction of PIP and PIP_2 with 15 μM U73122 and a reduction in the rate of incorporation of phosphate and glycerol; it proposes that U73122 may inhibit PI and PIP kinases and possibly also stimulate lipid phosphatases (Vickers, 1993). A patch-clamp study with pancreatic acinar cells shows that 10 μM U73122 can open plasma membrane ion channels and it can promote release of Ca^{2+} from intracellular stores (Mogami et al., 1997). They conclude that U73122 is not specific for PLC and mention the possibility of alkylation.

For U73122, our observations agree with strong inhibition of PLC, with a lack of specificity, and with some of the reported side effects. We find that a few micromolar U73122 blocks M_1 receptor coupling to PLC virtually completely in 1–2 min, confirming that the compound is an efficacious inhibitor of G protein–coupled PLC activation. At the same time, in a selected subset of our observations, U73122 initiates a slow decline of KCNQ2/3 current, a slow translocation of the PH-EGFP probe, a slow rise of intracellular Ca^{2+}, and in 5 min, a decrease of the PIP and PIP_2 pools of the cell. In RESULTS we presented the hypothesis that U73122 activates PLC to ~3% of its maximum activity while uncoupling signaling from G_q-coupled receptors. This hypothesis is consistent with the subset of results mentioned so far, but it does not explain for example why U73122 fails to induce a slow translocation of the C1-EGFP probe to the membrane. We can consider several alternative hypotheses. For example, inhibition of lipid kinases by U73122 (Vickers, 1993) would explain the translocation results, the decline of KCNQ2/3 current, and the fall of PIP and PIP_2 pools accompanied by a rise of PI; however, it does not explain the slow rise in Ca^{2+}. An activation of lipid phosphatases might look similar. Finally, the highly lipid-soluble cation U73122 might sequester anionic PIP_2 much as the lipid-soluble local anesthetic benzocaine has been proposed to inhibit PIP_2-sensitive GIRK K^+ channels by sequestering PIP_2 (Zhou et al., 2001). Sequestration of PIP_2 could lead to a decline of KCNQ2/3 current and a translocation of the PH-EGFP probe. Hydrophobic interactions might even release some C1-EGFP from the membrane if DAG is also sequestered by U73122. To speculate further, IP_3 receptors of the endoplasmic reticulum may be held in check by contact with PIP_2 on the plasma membrane (Lupu et al., 1998; Glouchankova et al., 2000), and if the available PIP_2 is reduced by sequestration, IP_3 receptors could become active, releasing Ca^{2+} from internal stores. Although it will not be anchored to proteins in the membrane by alkylation, the control compound U73343 is a hydrophobic cation as well and should share some of these effects, as it does weakly. The sequestration hypothesis does not explain why PIP and PIP_2 pool sizes fall with U73122. We feel that U73122 is a complex agent with multiple molecular actions, so it is not required that a single mechanism explain all the results. Perhaps all the mechanisms mentioned in this paragraph play some part in the overall effect.

Now we consider alkylation. U73122 and its control compound differ in that the active compound can alkylate and the control compound cannot. Our experiments comparing the two reactive maleimide compounds NEM and U73122 convince us that alkylation explains many side effects. There is a mutual mimicry or occlusion of effects. Either compound by itself quickly increases KCNQ2/3 currents, shifts their voltage dependence, and blocks $G_{i/o}$-coupled signaling to GIRK channels. Prior reaction with NEM prevents U73122 from either rapidly increasing KCNQ2/3 current or slowly decreasing it, and from inducing translocation of the PH-EGFP probe. Prior reaction with U73122 prevents NEM from augmenting KCNQ2/3 current. U73122 acts at 20-fold lower concentration than NEM, as might be expected for a maleimide with a lipophilic tether. When the reaction occurs, the entire aminosterol molecule (Fig. 2 A) will be coupled to the protein target, e.g., to the KCNQ channel subunit, or to $G\alpha_o$, etc. NEM may mimic U73122 in another respect. Longer exposures to NEM depress the pool of cellular PIP_2 and PIP, which might reflect inhibition of lipid kinases. For example, NEM and other sulfhydryl reagents block the stimulatory effects of ATP on ion transport activity that are now known to represent lipid kinase activity (Hilgemann and Collins, 1992).

A question we lack evidence about is whether U73122 alkylates PLC to inhibit it. We suggest that the answer is

yes, since block is irreversible and the control compound U73343 is not able to alkylate. However, although NEM slows receptor-coupled PLC (Fig. 5, A and D) it definitely does not stop it (in 2 min), and prior NEM does not prevent subsequent U73122 from fully arresting receptor-coupled PLC (Fig. 5 B). Thus 2.5–5 μM U73122 must react quickly with at least one cysteine of PLC that 100 μM NEM reacts with much more slowly or not at all. Perhaps the sterol moiety of U73122 guides it to this target.

The dose–response relation for U73122 action is often steep and seemingly variable. Several factors probably contribute to the variability: the compound is difficult to dissolve and needs vigorous vortexing in a hydrophobic vehicle; it precipitates from the stock solution in the refrigerator; maleimides are unstable once placed in water; and finally alkylation is irreversible, so there is no equilibrium binding. The reaction rate is likely to be directly proportional to the inhibitor concentration and fairly temperature dependent. Thus 20 min at 200 nM (Jin et al., 1994) is likely to be similar to 2 min at 2 μM, provided the temperature is the same. In brief, many factors make U73122 a difficult compound to work with. To avoid excessive side reactions, the product of concentration and duration of treatment should be kept as low as possible. In our hands edelfosine (ET-18-OCH_3) seemed a cleaner reagent although it was clearly cytotoxic and slow to act and may well have its own side effects.

Conclusions

We draw several conclusions. First, under a variety of new test conditions, the size of KCNQ current continues to be a consistent reporter of the cellular PIP_2 pool. Second, the strict Ca^{2+} dependence of receptor-activated PLCβ within the living cell subjects the enzyme both to strong positive feedback via its own IP_3 pathway and to strong enhancement by nearby coincident Ca^{2+} signaling in other systems. Third, the pharmacological tools for inhibiting and activating PLC must be used with caution. Fourth, the PIP_2 levels in cells transfected with M_1 muscarinic receptors undergo rapid and extensive depletion during receptor activation, whether monitored indirectly via KCNQ channel activity, fluorescent indicators of PIP_2 and DAG, or directly via total phosphoinositide measurements. Clearly, in the cell lines we used, receptor-activated PLCs have rapid access to the major PIP_2 pool of the cell. Work in other systems has suggested that the PIP_2 used in IP_3 signaling may instead be a small and highly compartmentalized pool of total cell PIP_2, a conclusion reached for example by using RNAi-mediated knock-down of individual lipid kinases (Wang et al., 2004). It remains to be seen how such contrasting impressions of PIP_2 signaling will be resolved.

APPENDIX

Diffusion of Probes into the Nucleus

An Elementary Model for Nuclear–Cytoplasmic Exchange of Probes. We observed that the translocation probes enter the nucleus slowly and recognized that this slow exchange would add transients to the measured values of cytoplasmic probe concentration. An elementary kinetic model was formulated to simulate the translocation of probes between plasma membrane, cytoplasm, and nucleus. The goal was to ask how adding the nuclear compartment alters the expected time course of cytoplasmic probe concentration changes.

In rough accord with images in Fig. 1 A, the cell was taken as a sphere with radius $r_C = 6$ μm, and the nucleus, as a sphere with radius $r_N = 4.4$ μm. This makes the area of the nuclear membrane $A_N = 273$ μm^2 and the volumes of the cytoplasm and nucleus, $V_C = 0.55$ pl and $V_N = 0.36$ pl, respectively. Flux F_{Pr} (units, mol s^{-1}) of probe from cytoplasm to nucleus was assumed to obey the standard passive permeability equation (Hille, 2001) $F_{Pr} = P_N A_N (Pr_C - Pr_N) * 10^{-15}$, where P_N is the nuclear membrane permeability to probe (units, μm s^{-1}), Pr_C and Pr_N are free cytoplasmic and nuclear probe concentrations (units, M), and 10^{-15} converts from liters to cubic micrometers. The rate of change of nuclear probe concentration would be $dPr_N/dt = F_{Pr}/V_N$ and similarly for the cytoplasmic concentration.

To simulate reversible release and binding of probe to a membrane ligand (e.g., to free PIP_2 or DAG lipid, L_f), the probe and lipid were assumed to undergo a conventional bimolecular reaction at the membrane with rate constants k_{on} and k_{off} (units, M^{-1} s^{-1} and s^{-1}), such that the rate of change of membrane-bound probe (Pr_M) is $dPr_M/dt = k_{on} Pr_C L_f - k_{off} Pr_M$. To avoid introducing surface concentration units, the lipid-bound probe and the free lipid are treated as though in solution throughout the cell volume, although both are actually only on the membrane. This has no effect on the calculated time courses but simplifies the units. In these units, the equilibrium dissociation constants ($K_d = k_{off}/k_{on}$) for the probe–lipid complexes were taken as 1.2 μM for PIP_2 and PH-EGFP and 3 μM for DAG and C1-EGFP. These apparent dissociation constants are overestimates in the sense that they do not take into account the possibility that most of the PIP_2 or DAG lipid may already be involved in other protein–lipid interactions. The known interaction of PH-EGFP with IP_3 was ignored, a shortcoming that has no influence on the nuclear–cytoplasmic exchange time that is the focus of the model. In the following section, K_ds for PH-EGFP are used in a much more complex model, and a lower K_d is needed for PIP_2 because there the IP_3 competition is included.

Finally, the ligand (PIP_2 or DAG lipid) was assumed to be produced at a rate k_{prod} (zeroeth order, M s^{-1}) and destroyed with a rate constant k_{dest} (first order, s^{-1}) so that the total rate of change of the free membrane lipid is $dL_f/dt = k_{prod} - k_{dest}L_f - dPr_M/dt$. The total amount of probe (0.5 μM) was set below the total amount of lipid (5 μM for PIP_2), so that binding to the probe would not strongly deplete the lipid. Activation of muscarinic receptor was simulated by increasing k_{dest} (for the PIP_2/IP_3 probe) or increasing k_{prod} (for the DAG probe) during the oxo-M application. The complete program for the model is available in the online supplemental material (available at http://www.jgp.org/cgi/content/full/jgp.200509309/DC1). The model was solved by Euler (first-order) integration using time steps of 25 ms in the Igor Pro programming environment (Wavemetrics).

Results of the Simple Exchange Model. Fig. 11 summarizes the main results after free parameters were manually adjusted to simulate the observations of Fig. 1 B. The model does simulate transients in the changes of cytoplasmic probe concentrations that continue well after the assumed lipid concentration changes brought on by agonist addition or removal are finished. Thus, PIP_2 is depleted during the two oxo-M applications, so the PH-EGFP probes translocate from the membrane to the cytoplasm, and then some of these probe molecules equilibrate into the nucleus (P_N = 0.0032 μm s^{-1}, exponential exchange time, τ ~281 s). Similarly, membrane DAG rises during oxo-M so the C1-EGFP probes translocate from the cytoplasm to the membrane, and additional probe molecules then equilibrate from the nucleus (P_N = 0.005 μm s^{-1}, exponential exchange time, τ ~188 s). The transients and the nuclear changes during onset and recovery resemble the measured time courses well enough to show that most if not all of the observed overshoots and decays can be understood as exchange of probe between cytoplasm and nucleus without postulating desensitizations and rebounds in the signaling from M_1 receptors.

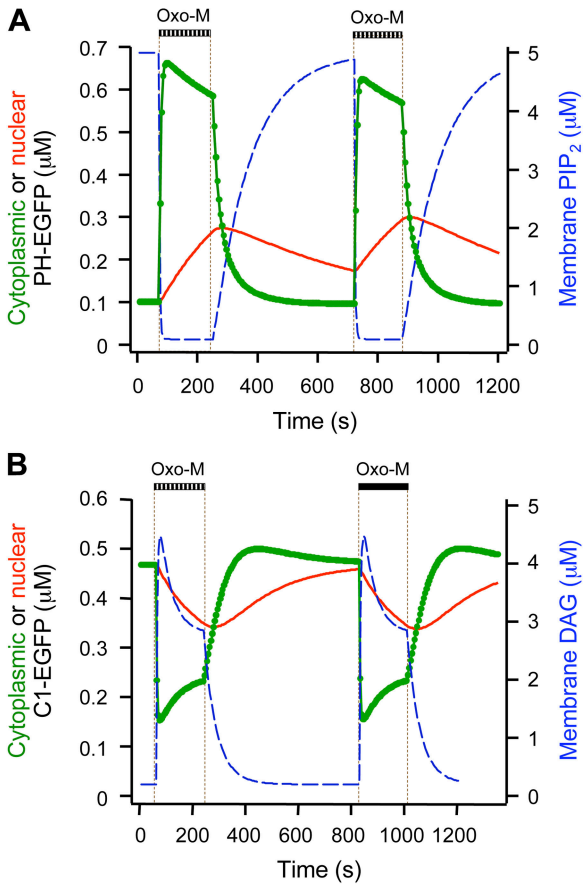

Figure 11. Elementary model of the exchange of optical probes between cytoplasmic and nuclear compartments. (A) Simulated time course of PIP_2 lipid (blue dashed line), cytoplasmic PH-EGFP (green symbols), and nuclear PH-EGFP (red line) during two applications of oxo-M. P_N = 0.0032 μm s^{-1}, k_{on} = 0.4 × 10^6 M^{-1} s^{-1}, k_{off} = 0.5 s^{-1}, initial L_f = 5 × 10^{-6} M, k_{prod} = 8.5 × 10^{-9} M s^{-1}, k_{dest} = 0.0085 s^{-1} at rest, and is 50 times higher during oxo-M treatment. Conditions chosen to mimic Fig. 1, B and C. (B) Simulated time course of DAG lipid (blue dashed line), cytoplasmic C1-EGFP (green circles), and nuclear C1-EGFP (red line) during two applications of oxo-M. P_N = 0.005 μm s^{-1}, k_{on} = 10^5 M^{-1} s^{-1}, k_{off} = 0.3 s^{-1}, initial L_f = 2.5 × 10^{-8} M, k_{prod} = 0.55 × 10^{-9} M s^{-1} at rest, and k_{dest} = 0.022 s^{-1}. During oxo-M stimulation, k_{prod} is multiplied by the time function, 14 + 140 * exp(−t/5), where t is time (units, s) after the beginning of the stimulus, simulating a burst of DAG production before PIP_2 is depleted.

Relationship of the PH Probe and C1 Probe Work to our Larger Kinetic Model of Phosphoinositide Metabolism

We discuss briefly the large kinetic model of Suh et al. (2004), which was tentatively formulated to describe muscarinic suppression of KCNQ current in 10–20 s, recovery of current after removal of agonist in ~200 s, and perturbation by cytoplasmic Mg^{2+} depletion and nucleotide analogs. That larger model was implemented in the Virtual Cell environment of the National Resource for Cell Analysis and Modeling, University of Connecticut Health Center (http://www.nrcam.uchc.edu). The revised working model with control values of rate constants and initial conditions is available at that web page for public use and modification.

In DISCUSSION we indicated a need to add cleavage of PIP by PLC to this model to account for the strong measured muscarinic depletion of PIP (Fig. 6). We consider here incorporating the translocation probes and the overexpression of the IP_3-phosphatase, IP_3-5-P, into the model. Since the model "cell" starts with 5 μM PIP_2 in the plasma membrane (referred to total cell volume), a sudden activation of PLC that hydrolyzes all the PIP_2 would produce 5 μM DAG and 5 μM IP_3. The PH probe binds to PIP_2 and IP_3 and the C1 probe binds

to DAG, a species not present in the original model. Therefore we added DAG as a species formed by PLC and added its breakdown/metabolism with a rate constant $k = 0.013\ s^{-1}$, chosen to produce a time constant of 75 s for decline of DAG after agonist withdrawal as in Fig. 1 G. The rate constant for IP_3 breakdown by endogenous IP_3-5-P was $k = 0.066\ s^{-1}$, chosen to produce a time constant of ~15 s for decline of IP_3 (not a value we measured).

Probes were assumed to be expressed at 0.5 μM concentration and to undergo reversible bimolecular interactions with their ligands. Published calorimetric measurements give dissociation constants K_d of 1.7 and 0.2 μM for the interactions of the PH domain with PIP_2 (in phospholipid vesicles) or IP_3 (in solution) (Lemmon et al., 1995), and surface plasmon assay measurements give 2.1 and 0.09 μM for the same ligands (Hirose et al., 1999). Calorimetry and plasmon assays give K_ds of 10 and 6 nM for the DAG interaction of the C1A domain of PKCγ (Ananthanarayanan et al., 2003). All these K_ds are expected to depend on the phospholipid composition of the vesicles used in the assay (Bittova et al., 2001).

Model simulations using the literature values for affinities of the PH domain gave a modest mimicry of the translocation seen in control cells. Half of the probe was bound to PIP_2 on the "plasma membrane" at rest and virtually all was released within 20 s of "oxo-M application." Then we tried to mimic the experiments with expression of IP_3-5-P. We slowed PLC 15-fold (to represent the absence of any Ca^{2+} rise) and speeded the IP_3-5-P in the model by 100-fold, which together reduced peak IP_3 accumulation below 30 nM. The modulation of KCNQ current and the appearance of DAG were slowed appropriately as in the experiments of Fig. 10 (C–F). However, unlike the experiment of Fig. 10 G, these changes did not prevent a strong translocation of PH domain to the cytoplasm during "oxo-M application." The problem was that the affinity of the PH probe for membrane PIP_2 was so low that any cleavage of PIP_2 would result in significant probe translocation. This was readily fixed by lowering the K_d for the PH domain–PIP_2 interaction 20-fold to 0.1 μM, approximately matching the K_d for IP_3. A related discrepancy with literature K_ds is revealed in published experiments determining what concentration of cytoplasmic IP_3 is needed to displace PH domain probes from the plasma membrane in intact cells. To displace half of the PH probe from the plasma membrane, Hirose et al. (1999) needed 13 μM IP_3 in MDCK cells, and Winks et al. (2005) needed 16 μM IP_3 in sympathetic neurons; and van der Wal et al. (2001) found that release of 10 μM IP_3 displaces only a small portion of the PH probe, 100 μM IP_3 displaces much more, and hydrolysis of PIP_2 induced by activation of bradykinin receptors displaces even more. Using the published K_ds in our large model predicted half release of PH domains already by 0.6 mM IP_3, quite unlike these experiments, whereas using the revised K_d for PIP_2 (0.1 μM) predicts half release by 7.8 μM IP_3. Thus the PIP_2 affinity in native membranes must be significantly higher than that in the phosphatidylcholine-phosphatidylserine vesicle environment used in binding assays. As an alternative approach, one might consider raising the PIP_2 concentration in the model from the chosen value of 5 μM (corresponding to 5,000 μm^{-2} in the plasma membrane for a cell of 0.6 μm^{-1} surface-to-volume ratio). However, this approach is inconsistent with the expected chemical content of the plasma membrane. If the inner leaflet of the plasma membrane is 50% lipid, there would be room for 700,000 phospholipid molecules per square micrometer. Raising the surface density of PIP_2 20-fold would make the inner leaflet 14% PIP_2. In conclusion, we consider that the effective in-cell K_ds of the PH probe for PIP_2 and IP_3 are about equal and near 0.1 μM.

Model simulations using the literature K_d values for the C1 domain were also not acceptable. The probe was fully associated with the plasma membrane rather than the cytoplasm in basal conditions because of its high affinity for the DAG formed there by the low, steady basal activity of PLC. The discrepancy could be fixed by raising the K_d 300-fold to 3 μM, which allowed 75% of the probe to be in the cytoplasm at rest. This might indicate that most of the basal DAG in the membrane is sequestered by other avid DAG-binding proteins (and the published K_d is correct) or that adding GFP to the C1 domain greatly reduces its DAG affinity. An alternative approach would be to slow the basal PLC rate drastically so that there is less basal DAG. In turn, that would require that PIP_2 synthesis in the model be made a regulated process with a basal rate reduced by the same factor as the basal PLC rate was reduced. We lack measurements of DAG and have no basis to make choices among these possibilities so far.

We thank Paulette Brunner and Greg Martin for help in the Keck Imaging Center, Stuart McLaughlin for discussion, and Lea Miller and Chengcheng Shen for expert technical assistance.

This work was supported by National Institutes of Health grants NS08174, AR17803, NS07332, DA00286, DA11322, and HL067942.

Olaf S. Andersen served as editor.

Submitted: 28 April 2005
Accepted: 19 July 2005

REFERENCES

Ananthanarayanan, B., R.V. Stahelin, M.A. Digman, and W. Cho. 2003. Activation mechanisms of conventional protein kinase C isoforms are determined by the ligand affinity and conformational flexibility of their C1 domains. *J. Biol. Chem.* 278:46886–

46894.

Bae, Y.S., T.G. Lee, J.C. Park, J.H. Hur, Y. Kim, K. Heo, J.Y. Kwak, P.G. Suh, and S.H. Ryu. 2003. Identification of a compound that directly stimulates phospholipase C activity. *Mol. Pharmacol.* 63: 1043–1050.

Bezprozvanny, I.B., K. Ondrias, E. Kaftan, D.A. Stoyanovsky, and B.E. Ehrlich. 1993. Activation of the calcium release channel (ryanodine receptor) by heparin and other polyanions is calcium dependent. *Mol. Biol. Cell.* 4:347–352.

Biddlecome, G.H., G. Berstein, and E.M. Ross. 1996. Regulation of phospholipase C-β1 by G_q and m1 muscarinic cholinergic receptor. Steady-state balance of receptor-mediated activation and GTPase-activating protein-promoted deactivation. *J. Biol. Chem.* 271:7999–8007.

Bittova, L., R.V. Stahelin, and W. Cho. 2001. Roles of ionic residues of the C1 domain in protein kinase C-α activation and the origin of phosphatidylserine specificity. *J. Biol. Chem.* 276:4218–4226.

Bleasdale, J.E., G.L. Bundy, S. Bunting, F.A. Fitzpatrick, R.M. Huff, F.F. Sun, and J.E. Pike. 1989. Inhibition of phospholipase C dependent processes by U-73,122. *Adv. Prostaglandin Thromboxane Leukot. Res.* 19:590–593.

Brown, D.A., and P.R. Adams. 1980. Muscarinic suppression of a novel voltage-sensitive K^+ current in a vertebrate neuron. *Nature.* 283:673–676.

Essen, L.O., O. Perisic, R. Cheung, M. Katan, and R.L. Williams. 1996. Crystal structure of a mammalian phosphoinositide-specific phospholipase Cδ. *Nature.* 380:595–602.

Fisher, S.K., L.M. Domask, and R.M. Roland. 1989. Muscarinic receptor regulation of cytoplasmic Ca^{2+} concentrations in human SK-N-SH neuroblastoma cells: Ca^{2+} requirements for phospholipase C activation. *Mol. Pharmacol.* 35:195–204.

Ford, C.P., P.L. Stemkowski, and P.A. Smith. 2004. Possible role of phosphatidylinositol 4,5 bisphosphate in luteinizing hormone releasing hormone-mediated M-current inhibition in bullfrog sympathetic neurons. *Eur. J. Neurosci.* 20:2990–2998.

Glouchankova, L., U.M. Krishna, B.V. Potter, J.R. Falck, and I. Bezprozvanny. 2000. Association of the inositol (1,4,5)-trisphosphate receptor ligand binding site with phosphatidylinositol (4,5)-bisphosphate and adenophostin A. *Mol. Cell Biol. Res. Commun.* 3:153–158.

Hashimotodani, Y., T. Ohno-Shosaku, H. Tsubokawa, H. Ogata, K. Emoto, T. Maejima, K. Araishi, H.S. Shin, and M. Kano. 2005. Phospholipase Cβ serves as a coincidence detector through its Ca^{2+} dependency for triggering retrograde endocannabinoid signal. *Neuron.* 45:257–268.

Hilgemann, D.W., and A. Collins. 1992. Mechanism of cardiac Na^+-Ca^{2+} exchange current stimulation by MgATP: possible involvement of aminophospholipid translocase. *J. Physiol.* 454:59–82.

Hilgemann, D.W., S. Feng, and C. Nasuhoglu. 2001. The complex and intriguing lives of PIP_2 with ion channels and transporters. *Sci. STKE.* 111:RE19.

Hille, B. 2001. Ion Channels of Excitable Membranes. Third edition. Sinauer Associates, Sunderland, MA. 444 pp.

Hirdes, W., L.F. Horowitz, and B. Hille. 2004. Muscarinic modulation of erg potassium current. *J. Physiol.* 559:67–84.

Hirose, K., S. Kadowaki, M. Tanabe, H. Takeshima, and M. Iino. 1999. Spatiotemporal dynamics of inositol 1,4,5-trisphosphate that underlies complex Ca^{2+} mobilization patterns. *Science.* 284: 1527–1530.

Jansen, S., J. Arning, D. Kemken, T. Dulcks, and D. Beyersmann. 2004. Phospholipase C activator 2,4,6-trimethyl-N-(meta-3-trifluoromethyl-phenyl)-benzene-sulfonamide decays under ultraviolet light and shows strong self-fluorescence. *Anal. Biochem.* 330:353–355.

Jin, W., T.M. Lo, H.H. Loh, and S.A. Thayer. 1994. U73122 inhibits phospholipase C-dependent calcium mobilization in neuronal cells. *Brain Res.* 642:237–243.

Kim, Y.H., T.J. Park, Y.H. Lee, K.J. Baek, P.G. Suh, S.H. Ryu, and K.T. Kim. 1999. Phospholipase C-δ1 is activated by capacitative calcium entry that follows phospholipase C-β activation upon bradykinin stimulation. *J. Biol. Chem.* 274:26127–26134.

Krjukova, J., T. Holmqvist, A.S. Danis, K.E. Akerman, and J.P. Kukkonen. 2004. Phospholipase C activator *m*-3M3FBS affects Ca^{2+} homeostasis independently of phospholipase C activation. *Br. J. Pharmacol.* 143:3–7.

Lemmon, M.A. 2003. Phosphoinositide recognition domains. *Traffic.* 4:201–213.

Li, Y., N. Gamper, and M.S. Shapiro. 2004. Single-channel analysis of KCNQ K^+ channels reveals the mechanism of augmentation by a cysteine-modifying reagent. *J. Neurosci.* 24:5079–5090.

Lemmon, M.A., K.M. Ferguson, R. O'Brien, P.B. Sigler, and J. Schlessinger. 1995. Specific and high-affinity binding of inositol phosphates to an isolated pleckstrin homology domain. *Proc. Natl. Acad. Sci. USA.* 92:10472–10476.

Lupu, V.D., E. Kaznacheyeva, U.M. Krishna, J.R. Falck, and I. Bezprozvanny. 1998. Functional coupling of phosphatidylinositol 4,5-bisphosphate to inositol 1,4,5-trisphosphate receptor. *J. Biol. Chem.* 273:14067–14070.

Mogami, H., C.L. Mills, and D.V. Gallacher. 1997. Phospholipase C inhibitor, U73122, releases intracellular Ca^{2+}, potentiates $Ins(1,4,5)P_3$-mediated Ca^{2+} release and directly activates ion channels in mouse pancreatic acinar cells. *Biochem. J.* 324:645–651.

Nasuhoglu, C., S. Feng, J. Mao, M. Yamamoto, H.L. Yin, S. Earnest, B. Barylko, J.P. Albanesi, and D.W. Hilgemann. 2002a. Nonradioactive analysis of phosphatidylinositides and other anionic phospholipids by anion-exchange high-performance liquid chromatography with suppressed conductivity detection. *Anal. Biochem.* 301:243–254.

Nasuhoglu, C., S. Feng, Y. Mao, I. Shammat, M. Yamamato, S. Earnest, M. Lemmon, and D.W. Hilgemann. 2002b. Modulation of cardiac PIP_2 by cardioactive hormones and other physiologically relevant interventions. *Am. J. Physiol. Cell Physiol.* 283:C223–C234.

Oancea, E., M.N. Teruel, A.F. Quest, and T. Meyer. 1998. Green fluorescent protein (GFP)-tagged cysteine-rich domains from protein kinase C as fluorescent indicators for diacylglycerol signaling in living cells. *J. Cell Biol.* 140:485–498.

Okubo, Y., S. Kakizawa, K. Hirose, and M. Iino. 2004. Cross talk between metabotropic and ionotropic glutamate receptor-mediated signaling in parallel fiber-induced inositol 1,4,5-trisphosphate production in cerebellar Purkinje cells. *J. Neurosci.* 24: 9513–9520.

Pfaffinger, P.J., J.M. Martin, D.D. Hunter, N.M. Nathanson, and B. Hille. 1985. GTP-binding proteins couple cardiac muscarinic receptors to a K^+ channel. *Nature.* 317:536–538.

Powis, G., M.J. Seewald, C. Gratas, D. Melder, J. Riebow, and E.J. Modest. 1992. Selective inhibition of phosphatidylinositol phospholipase C by cytotoxic ether lipid analogues. *Cancer Res.* 52: 2835–2840.

Rhee, S.G. 2001. Regulation of phosphoinositide-specific phospholipase C. *Annu. Rev. Biochem.* 70:281–312.

Roche, J.P., R. Westenbroek, A.J. Sorom, B. Hille, K. Mackie, and M.S. Shapiro. 2002. Antibodies and a cysteine-modifying reagent show correspondence of M current in neurons to KCNQ2 and KCNQ3 K^+ channels. *Br. J. Pharmacol.* 137:1173–1186.

Rohrbough, J., and K. Broadie. 2005. Lipid regulation of the synaptic vesicle cycle. *Nat. Rev. Neurosci.* 6:139–150.

Ryu, S.H., K.S. Cho, K.Y. Lee, P.G. Suh, and S.G. Rhee. 1987a. Purification and characterization of two immunologically distinct phosphoinositide-specific phospholipases C from bovine brain. *J.*

Biol. Chem. 262:12511–12518.

Ryu, S.H., P.G. Suh, K.S. Cho, K.Y. Lee, and S.G. Rhee. 1987b. Bovine brain cytosol contains three immunologically distinct forms of inositolphospholipid-specific phospholipase C. *Proc. Natl. Acad. Sci. USA.* 84:6649–6653.

Shapiro, M.S., J.P. Roche, E.J. Kaftan, H. Cruzblanca, K. Mackie, and B. Hille. 2000. Reconstitution of muscarinic modulation of the KCNQ2/KCNQ3 K^+ channels that underlie the neuronal M current. *J. Neurosci.* 20:1710–1721.

Shapiro, M.S., L.P. Wollmuth, and B. Hille. 1994. Modulation of Ca^{2+} channels by PTX-sensitive G-proteins is blocked by N-ethylmaleimide in rat sympathetic neurons. *J. Neurosci.* 14:7109–7116.

Smith, R.J., L.M. Sam, J.M. Justen, G.L. Bundy, G.A. Bala, and J.E. Bleasdale. 1990. Receptor-coupled signal transduction in human polymorphonuclear neutrophils: effects of a novel inhibitor of phospholipase C-dependent processes on cell responsiveness. *J. Pharmacol. Exp. Ther.* 253:688–697.

Smrcka, A.V., J.R. Hepler, K.O. Brown, and P.C. Sternweis. 1991. Regulation of polyphosphoinositide-specific phospholipase C activity by purified G_q. *Science.* 251:804–807.

Stauffer, T.P., S. Ahn, and T. Meyer. 1998. Receptor-induced transient reduction in plasma membrane PtdIns(4,5)P_2 concentration monitored in living cells. *Curr. Biol.* 8:343–346.

Stemkowski, P.L., F.W. Tse, V. Peuckmann, C.P. Ford, W.F. Colmers, and P.A. Smith. 2002. ATP-inhibition of M current in frog sympathetic neurons involves phospholipase C but not Ins P_3, Ca^{2+}, PKC, or Ras. *J. Neurophysiol.* 88:277–288.

Suh, B.C., and B. Hille. 2002. Recovery from muscarinic modulation of M current channels requires phosphatidylinositol 4,5-bisphosphate synthesis. *Neuron.* 35:507–520.

Suh, B.C., and B. Hille. 2005. Regulation of ion channels by phosphatidylinositol 4,5,-bisphosphate. *Curr. Opin. Neurobiol.* 15:370–378.

Suh, B.C., L.F. Horowitz, W. Hirdes, K. Mackie, and B. Hille. 2004. Regulation of KCNQ2/KCNQ3 current by G protein cycling: the kinetics of receptor-mediated signaling by G_q. *J. Gen. Physiol.* 123: 663–683.

van der Wal, J., R. Habets, P. Varnai, T. Balla, and K. Jalink. 2001. Monitoring agonist-induced phospholipase C activation in live cells by fluorescence resonance energy transfer. *J. Biol. Chem.* 276:15337–15344.

Várnai, P., and T. Balla. 1998. Visualization of phosphoinositides that bind pleckstrin homology domains: calcium- and agonist-induced dynamic changes and relationship to *myo*-[^{3}H]inositol-labeled phosphoinositide pools. *J. Cell Biol.* 143:501–510.

Vickers, J.D. 1993. U73122 affects the equilibria between the phosphoinositides as well as phospholipase C activity in unstimulated and thrombin-stimulated human and rabbit platelets. *J. Pharmacol. Exp. Ther.* 266:1156–1163.

Wang, Y.J., W.H. Li, J. Wang, K. Xu, P. Dong, X. Luo, and H.L. Yin. 2004. Critical role of PIP5KIγ87 in $InsP_3$-mediated Ca^{2+} signaling. *J. Cell Biol.* 167:1005–1010.

Wei, X., V.G. Henke, C. Strubing, E.B. Brown, and D.E. Clapham. 2003. Real-time imaging of nuclear permeation by EGFP in single intact cells. *Biophys. J.* 84:1317–1327.

Willars, G.B., S.R. Nahorski, and R.A. Challiss. 1998. Differential regulation of muscarinic acetylcholine receptor-sensitive polyphosphoinositide pools and consequences for signaling in human neuroblastoma cells. *J. Biol. Chem.* 273:5037–5046.

Wilson, D.B., T.E. Bross, S.L. Hofmann, and P.W. Majerus. 1984. Hydrolysis of polyphosphoinositides by purified sheep seminal vesicle phospholipase C enzymes. *J. Biol. Chem.* 259:11718–11724.

Winks, J.S., S. Hughes, A.K. Filippov, L. Tatulian, F.C. Abogadie, D.A. Brown, and S.J. Marsh. 2005. Relationship between membrane phosphatidylinositol-4,5-bisphosphate and receptor-mediated inhibition of native neuronal M channels. *J. Neurosci.* 25: 3400–3413.

Wojcikiewicz, R.J., A.B. Tobin, and S.R. Nahorski. 1994. Muscarinic receptor-mediated inositol 1,4,5-trisphosphate formation in SH-SY5Y neuroblastoma cells is regulated acutely by cytosolic Ca^{2+} and by rapid desensitization. *J. Neurochem.* 63:177–185.

Xu, C., J. Watras, and L.M. Loew. 2003. Kinetic analysis of receptor-activated phosphoinositide turnover. *J. Cell Biol.* 161:779–791.

Yin, H.L., and P.A. Janmey. 2003. Phosphoinositide regulation of the actin cytoskeleton. *Annu. Rev. Physiol.* 65:761–789.

Zhang, H., L.C. Craciun, T. Mirshahi, T. Rohacs, C.M. Lopes, T. Jin, and D.E. Logothetis. 2003. PIP_2 activates KCNQ channels, and its hydrolysis underlies receptor-mediated inhibition of M currents. *Neuron.* 37:963–975.

Zhou, W., C. Arrabit, S. Choe, and P.A. Slesinger. 2001. Mechanism underlying bupivacaine inhibition of G protein-gated inwardly rectifying K^+ channels. *Proc. Natl. Acad. Sci. USA.* 98:6482–6487.